ADVANCING EARTH AND SPACE SCIENCES

JGR Planets

RESEARCH ARTICLE

10.1029/2026JE009650

**Key Points:**

- Bimodal size distributions of scoriaceous and unmelted micrometeorites are larger than cosmic spherules, indicating ~87% entry mass loss
- The bimodality of the size distribution reflects contrasting lithological end-member components (fine- and coarse-grained micrometeorites)
- The pre-atmospheric mass flux over the Quaternary is ~12 kt/yr, indicating that the influx has remained stable in the last few million years

**Supporting Information:**

Supporting Information may be found in the online version of this article.

**Correspondence to:**

S. Ottaviani,
samuele.ottaviani@dottorandi.unipg.it

**Citation:**

Ottaviani, S., Folco, L., Suttle, M. D., Repič, R., Mancini, L., Battiston, T., et al. (2026). Cosmic dust flux during the quaternary: The record of large scoriaceous and unmelted micrometeorites from the transantarctic mountains collection. *Journal of Geophysical Research: Planets*, *131*, e2026JE009650. https://doi.org/10.1029/2026JE009650

Received 13 JAN 2026
Accepted 22 JUN 2026



# Cosmic Dust Flux During the Quaternary: The Record of Large Scoriaceous and Unmelted Micrometeorites From the Transantarctic Mountains Collection

**S. Ottaviani[1,2], L. Folco[1,3], M. D. Suttle[1,4], R. Repič[5], L. Mancini[5], T. Battiston[5], S. Iannini Lelarge[1,6], and M. Masotta[1,3]**

[1]Dipartimento di Scienze della Terra, Università di Pisa, Pisa, Italy, [2]Dipartimento di Fisica e Geologia, Università degli Studi di Perugia, Perugia, Italy, [3]CISUP, Centro per l'Integrazione della Strumentazione dell'Università di Pisa, Pisa, Italy, [4]School of Physical Sciences, The Open University, Milton Keynes, UK, [5]Slovenian National Building and Civil Engineering Institute - ZAG, Ljubljana, Slovenia, [6]Consiglio Nazionale delle Ricerche, Istituto di Geoscienze e Georisorse, Pisa, Italy

**Abstract** We estimate the cosmic dust flux to Earth through the study of rare micrometeorites that preserve part of their precursor features during atmospheric entry heating, namely unmelted and scoriaceous subtypes. Combining high-precision mass balance measurements, X-ray computed microtomography and scanning electron microscopy, we studied mass, size and petrography of 207 micrometeorites recovered from sediment traps in the Transantarctic Mountains (TAM), ranging from ~170 to ~1650 μm. Chondrules were identified in ~14% of the micrometeorites, particularly among coarse-grained and composite particles. The analysed population shows a bimodal size-frequency distribution, with peaks at ~305 μm and ~470 μm. A similar bimodal distribution was previously reported from the TAM cosmic spherule population, yet shifted towards lower sizes. This size-shift is consistent with an average mass loss of ~87% during atmospheric entry heating. The mass-size relationship follows a power-law, where the spherical equivalent diameter ($d_{\mu m}$) and mass ($m_{\mu g}$) of the micrometeorite are related by: $m = 1.07 \times 10^{-6} d^{2.96}$. The size-frequency distribution of the fine- and coarse-grained micrometeorites reveals two well-separated clusters, with peaks at ~315 μm and ~550 μm, respectively. These observations suggest that the bimodal distribution in the micrometeorite flux reflects contrasting lithological end-member components with different physical properties and fragmentation behaviours during dust production in space. Based on earlier mass flux estimates from TAM melted micrometeorites and accounting for the mass loss due to atmospheric entry derived here, we calculate a time-averaged pre-atmospheric mass flux of ~12,000 (±6,000) t/yr over the Quaternary, suggesting that the influx has remained stable over the last few million years.

**Plain Language Summary** Every day, large amounts of micrometre- to millimetre-sized extraterrestrial dust reach Earth. Most particles melt during atmospheric entry heating and arrive at the surface as cosmic spherules, while a smaller fraction survives and retains pre-atmospheric properties; these are known as unmelted and scoriaceous micrometeorites. We studied 207 unmelted and scoriaceous particles recovered from the Transantarctic Mountains (TAM). Their size distribution shows two main populations, with peaks at approximately 305 μm and 470 μm. A similar bimodal pattern was previously identified in TAM cosmic spherules, but shifted toward smaller sizes. This difference suggests that particles lose most of their original mass (~87%) during complete melting in atmospheric entry. Fine-grained and coarse-grained micrometeorites also form distinct size clusters, reflecting differences in the physical properties and fragmentation behaviour of their precursor materials. We estimated the total cosmic dust flux entering Earth's atmosphere by combining previous flux estimates from TAM cosmic spherules with the inferred mass loss during entry. The resulting pre-atmospheric flux is ~12 kt per year, suggesting that the influx of cosmic dust to Earth has remained relatively stable over the last few million years.

## 1. Introduction

Micrometeorites are interplanetary dust particles captured by the Earth's gravitational field and recovered at the Earth's surface. Surviving the hypervelocity impact with the Earth's upper atmosphere, they reach the Earth's surface where they are recovered as particles typically ranging from 10 μm to about 2 mm in size (Rubin & Grossman, 2010). Interplanetary dust is mainly produced by collisions among solid bodies and by surface sublimation of icy bodies, including primitive objects like asteroids and comets, and possibly terrestrial planets and their moons (Genge et al., 2008; Noguchi et al., 2015; Suavet et al., 2010).

Through the combined effects of Poynting–Robertson drag and gravitational focusing (Dermott et al., 2001; Marzari & Vanzani, 1994), interplanetary dust particles follow spiral trajectories toward the inner Solar System, where they are predominantly consumed by the Sun. However, a non-negligible fraction is intercepted by the terrestrial planets. This process results in an annual influx previously estimated at ∼40,000 ± 20,000 tonnes of micrometeoroids that hit the Earth's upper atmosphere (Love & Brownlee, 1993). The study of micrometeorites offers insights into the origin and geologic evolution of their parent bodies (e.g., Nava et al., 2020), modelling the origin and dynamic evolution of the cosmic dust complex in the near-Earth space (e.g., Carrillo-Sánchez et al., 2016) and their contribution to the global geochemical budget of planet Earth, including its bearing on the emergence of life (e.g., Walton et al., 2024).

Micrometeorites are classified according to the degree of melting experienced during atmospheric entry heating into three groups: melted micrometeorites or cosmic spherules, partially melted scoriaceous micrometeorites, and unmelted micrometeorites (Genge et al., 2008). The degree of atmospheric heating is influenced by several parameters, including entry velocity, size, chemistry, density, porosity and entry angle of the micrometeoroid (Briani et al., 2013; Flynn, 2001; Love & Brownlee, 1991). The survival of large micrometeorites with limited melting requires particularly favourable entry conditions. Most large particles are therefore expected to undergo substantial melting during atmospheric entry and are more commonly recovered as cosmic spherules. The unmelted and scoriaceous micrometeorites considered in this study thus represent a relatively rare subset of the incoming flux. About 10% of cosmic dust particles collected at the Earth's surface are unmelted or scoriaceous, thus preserving, at least in part, primary features of their parent bodies (Suttle & Folco, 2020; van Ginneken et al., 2012, van Ginneken et al., 2024, Van Maldeghem et al., 2023). Previous studies have shown that, for the largest size fractions of cosmic dust (>400 μm), the overall petrography and textures of these particles closely reflect those of their respective precursors (Badyukov et al., 2018; Genge et al., 2008; Gounelle et al., 2009; Suttle, Folco, et al., 2019; Suttle et al., 2020; van Ginneken et al., 2012; Van Maldeghem et al., 2023). Consequently, unmelted micrometeorites are a valuable source of information for accurate statistics about interplanetary dust source bodies.

A significant accumulation of micrometeorites was discovered by a research team of the Italian *Programma Nazionale delle Ricerche in Antartide* (PNRA) on the Myr-old summits of several isolated nunataks in the Victoria Land Transantarctic Mountains (TAM) during the 2003 expedition (Rochette et al., 2008). Since then, several collection campaigns have been undertaken by PNRA teams, which led to the recovery of tens of thousands of micrometeorites. The TAM micrometeorites are found in loose subaerial sediments, accumulated within joints and weathering pits on flat glacially eroded summit plateaus of Miocene age. Their characterization has documented that the collection samples the flux of cosmic dust to Earth over the last ∼1–2 million years (Rochette et al., 2008; Suttle & Folco, 2020; i.e., 1–2 orders of magnitude longer than most of the well-characterised micrometeorite collection sites). The TAM collection contains many thousands of individual particles up to 3 mm in size, with an abundance of otherwise rare unmelted and large micrometeorites (Dionnet et al., 2020; Suavet et al., 2009; Suttle, Folco, et al., 2019; Suttle, Genge, et al., 2019; Suttle et al., 2020; van Ginneken et al., 2012). The TAM micrometeorite collection offers a distinct opportunity to obtain a time-averaged estimate of the flux of micrometeorites over the last few million years, in terms of both parentage and mass.

Previous studies based on chemical and isotopic composition of totally melted cosmic spherules have also shown that particle size is closely related to parent body type (Cordier & Folco, 2014; Suavet et al., 2010; Suttle & Folco, 2020): dust from primitive objects such as C-, D-, and P-type asteroids in the outer belt and comets are proportionally more abundant in the smaller size fractions, whereas dust from more evolved and differentiated bodies, including S- and V-type asteroids in the inner belt, dominate among coarser size fractions. Available estimates of the cosmic dust flux to Earth, in terms of total mass, size, composition and parent body type, are limited to populations comprising relatively small micrometeorites, typically <400 μm in size and to micrometeorites that lost virtually the totality of their primary petrographic features (mineral composition and textures) through total melting during entry (i.e., cosmic spherules; e.g., Suavet et al., 2009; Prasad et al., 2013; Suttle & Folco, 2020; Rojas et al., 2021). Consequently, our understanding of the composition of the inner Solar System interplanetary dust complex remains incomplete. We therefore investigated large unmelted and scoriaceous micrometeorites, which better preserve their primary mineralogical and textural characteristics, studying a

**Table 1**
*Sampling Sites, Number Per Type and Size Range of the Transantarctic Mountains Micrometeorites Studied in This Work.*

| Sampling sites | | | | | | Micrometeorites[b] | | | | | | | | |
|---|---|---|---|---|---|---|---|---|---|---|---|---|---|---|
| Locality | Lat S | Long E | Elevation (*m*) | Bedrock[a] | | UnCg (*n*) | UnFg (*n*) | ScCg (*n*) | ScFg (*n*) | UnCom (*n*) | ScCom (*n*) | Total (*n*) | Size range (μm) | Mass range (μg) |
| Allan Hills | 76°44.733' | 159°23.023 | 2000 | Ignimbrite MF | | 3 | 2 | | | | | 5 | 311–775 | 34–509 |
| Elephant Moraine | 76°19.421' | 157°12.451 | 2100 | Moraine (BS-FD) | | | | | | | 1 | 1 | 592 | 143 |
| Killer Nunatak | 71°54.213' | 160°29.337 | 2080 | Granitoids GHI | | | | 4 | | | 1 | 5 | 479–784 | 146–465 |
| Miller Butte | 72°42.751' | 160°11.994' | 2600 | Granitoids GHI | | 45 | 26 | 5 | 71 | 4 | 11 | 162 | 168–1652 | 8–4181 |
| Oona Cliff | 72°25.988' | 160°06.638' | 2160 | Granitoids GHI | | | | | 1 | | | 1 | 234 | 12 |
| Pian delle Tectiti | 74°11.013' | 162°14.375' | 3000 | Granitoids GHI | | 2 | 3 | 1 | 6 | | | 12 | 384–830 | 79–531 |
| Schroeder Spur | 71°39.814' | 160°19.291 | 1800 | Granitoids GHI | | 3 | 4 | | 14 | | | 21 | 215–674 | 10–337 |
| | | | | | Total (*n*) | 53 | 35 | 10 | 92 | 4 | 13 | 207 | | |

[a]MF = Mawson Formation; BS = Beacon Supergroup; FD = Ferrar Dolerite; GHI = Granite Harbour Intrusive. [b]UnCg = Unmelted Coarse-grained; UnFg = Unmelted Fine-grained; ScCg = Scoriaceous Coarse-grained; ScFg = Scoriaceous Fine-grained; UnCom = Unmelted Composite; ScCom = Scoriaceous Composite.

statistically significant number ($N = 207$) of TAM unmelted and scoriaceous micrometeorites in the ∼170–1,650 μm size range. This study complements the previous assessment of micrometeorite size distribution, which was based on totally melted TAM cosmic spherules (Suavet et al., 2009; Suttle & Folco, 2020) for a more accurate definition of the micrometeorites flux reaching Earth during the Quaternary.

## 2. Materials and Methods

### 2.1. Samples

The 207 micrometeorites studied in this work (Table 1) comprise 70% of the entire population of the scoriaceous and unmelted micrometeorites belonging to the TAM collection, having been extracted from the host sediments during the selection of other types of extraterrestrial particles like cosmic spherules or airburst debris for other studies (e.g., Cordier et al., 2011, 2012; van Ginneken et al., 2010, 2012) since its discovery in 2003 (Rochette et al., 2008). The studied micrometeorites were collected in Victoria Land TAM during the 2003, 2006, 2009, 2012, 2014, and 2017 Antarctic field seasons of the Italian PNRA.

The great majority of the studied micrometeorites are from sediment traps occurring on summit plateaus of nunataks, as described in detail by Rochette et al., 2008; Folco et al., 2008; Suttle & Folco, 2020. From North to South (Figure 1), they are: Schroeder Spur, Killer Nunatak, Oona Cliff, Miller Butte, Pian delle Tectiti (in the catchment of the Reeves Glacier). These nunataks are virtually ice-free and consist of felsic granitoids belonging to the Paleozoic Granite Harbour Intrusive Complex (GANOVEX III, 1987). Their flat tops, presently some to several hundred meters above the ice level, record the glacial erosive action (e.g., polishes, striae, whale backs, crescents) of an overriding Neogene icesheet (e.g., Höfle, 1989; van der Wateren et al., 1996, 1999). Exposure ages of surface in the region obtained through $^{10}$Be, $^{26}$Al, and $^{3}$He cosmogenic nuclide analyses range from 2.3 (Mount Bowers; a few km due N of Miller Butte; van der Wateren et al., 1996) to 4 million years (Frontier Mountain; ∼30 km due SSW of Miller Butte; Rochette et al., 2008; Welten et al., 2008). Cracks, joints and weathering pits on this surface are filled with a gritty loose sediment (regolith) derived from the erosion of the granitoid bedrock, providing the geological setting for the accumulation of cosmic dust fallout over the last 1–2 million years (Rochette et al., 2008; Suttle & Folco, 2020). This long accumulation time is documented by the ubiquitous occurrence in the sediment of ∼0.8 million years old Australasian microtektites (Folco et al., 2008, 2009) and cosmic spherules recording inverse polarity (Suavet et al., 2011).

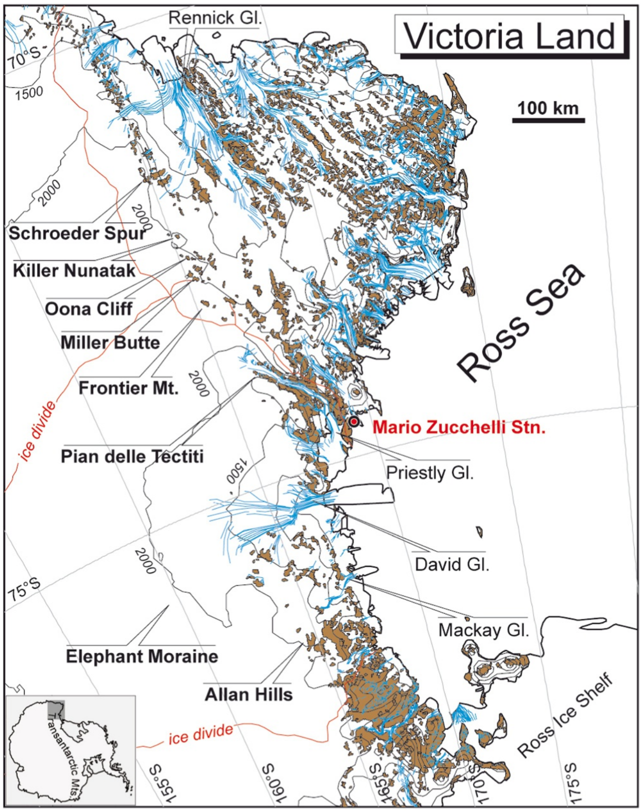


**Figure 1.** Sketch map of Victoria Land - Ross Sea Embayment (Antarctica) showing the eight locations where the Transantarctic Mountains micrometeorites studied in this work were collected from: Allan Hills, Elephant Moraine, Killer Nunatak, Miller Butte, Oona Cliff, Pian delle Tectiti and Schroeder Spur. Brown areas represent exposed bedrock; blue lines show ice flow; red lines mark ice-divides, black lines are contour lines. Inset: location map.

Additionally, five micrometeorites are from sediment traps located at the top of a low-relief glacially eroded crest protruding through the Allan Hills ice-field, in the catchment of the Mackay-David Glaciers. The crest sampled at Allan Hills consists of ignimbrites belonging to the Early Jurassic Mawson Formation. It forms a low-relief barrier ~20 m above ice level to the north-northeastward ice flow of the ice sheet towards the Mackay Glacier (Folco et al., 2016; Schultz et al., 1990). Its rounded crest is evidence of glacial overriding in the past. Based on cosmogenic nuclides denudation ages (Nishiizumi et al., 1991), Allan Hills have been exposed above the present ice surface for more than a half-million years, and the occurrence of Australasian microtektites in the same sediment traps suggests denudation – and thus fall out accumulation – for over 800,000 years (Folco et al., 2016). One micrometeorite studied here is from the supraglacial moraine in the Elephant Moraine ice field, in the catchment of the Mackay-David Glaciers. Micrometeorites were found within the fines of the rock veneer of the moraine which consists predominantly of Jurassic Ferrar dolerite and Devonian to Triassic Beacon supergroup sedimentary rocks (Cassidy et al., 1992). No information about the accumulation time is available for this site.

The sediment samples from all the micrometeorite traps considered in this work were dried using vacuum pumping and subsequently dry-sieved through the following meshes: 2,000, 800, 400, 200, and 100 μm. Scoriaceous and unmelted micrometeorites were identified due to their characteristic appearance, i.e. dark-grey colour and scoriaceous to angular shapes and extracted from the host detritus under a stereomicroscope. Their extraterrestrial origin was then confirmed through backscattered electron imaging of whole particles under a field-emission gun - scanning electron microscope.

### 2.2. Analytical Techniques

Micrometeorites were washed in an ultrasonic bath using deionized water, dried under vacuum, and weighed using a Mettler-Toledo XP6 microbalance (readability: 1 μg). They were then sorted by size and mounted on fifteen 10-mm-diameter Al-stubs, C-coated and imaged under a field-emission gun – scanning electron microscope (FEG-SEM) FEI Quanta 450 at the CISUP (*Centre for Instrument Sharing of the University of Pisa*, *Pisa*, *Italy*), in order to define their mass and size, respectively. The studied micrometeorites have irregular shapes, although many are rounded. The backscattered (BSE) images (Figure 2) were primarily employed as a means to observe textural criteria for characterisation and classification of the micrometeorites (e.g., the presence of magnetite rims, vesicles and dehydration cracks, scoriaceous structures, angular to sub-rounded and lobate morphologies, characteristic weathering products such as weathering encrustation rims and Na-S-rich salt deposits), as defined in Genge et al. (2008), Folco and Cordier (2015) and van Ginneken et al. (2016). Running conditions were: 5 to 15 kV accelerating voltage, 1 μm nominal beam spot size, variable working distance from 5 to 15 mm, unmonitored beam current and high-vacuum mode (~$10^{-5}$ mbar).

In order to analyse particle morpho-textural features in the 3D domain and ensure high confidence in classification, all samples in the studied collection were characterised using a non-destructive imaging approach based on X-ray computed microtomography (μXCT; Figure 3). These measurements were performed using a RX Solutions EasyTom XL 160/230 Ultra scanner, available at ZAG (*Slovenian National Building and Civil Engineering Institute*, *Ljubljana*, *Slovenia*). Given the large number of micrometeorites under study, runs were conducted on batches of 10-20 micrometeorites mounted on 10-mm-diameter Al-stub used for previous SEM investigations. To be able to distinguish most of the textural features of the samples, an effective pixel size of 3.00 × 3.00 $\mu m^2$ (working in extended field of view and propagation-based phase contrast modes) was employed in the μXCT scanning. Each sample was scanned using an open transmission nanofocus source, operating with a W filament, and a 16-bit, 2,560 × 2,048 pixels flat panel detector with an active area of 31.74 × 25.39 $cm^2$. The following acquisition conditions were applied: a voltage from 100 to 130 $kV_p$, an aluminium filter with thickness from 1.2 to 1.7 mm, a current of 200 μA, an exposure time of 1 frame/sec. A set of 4000 projections was acquired over a total

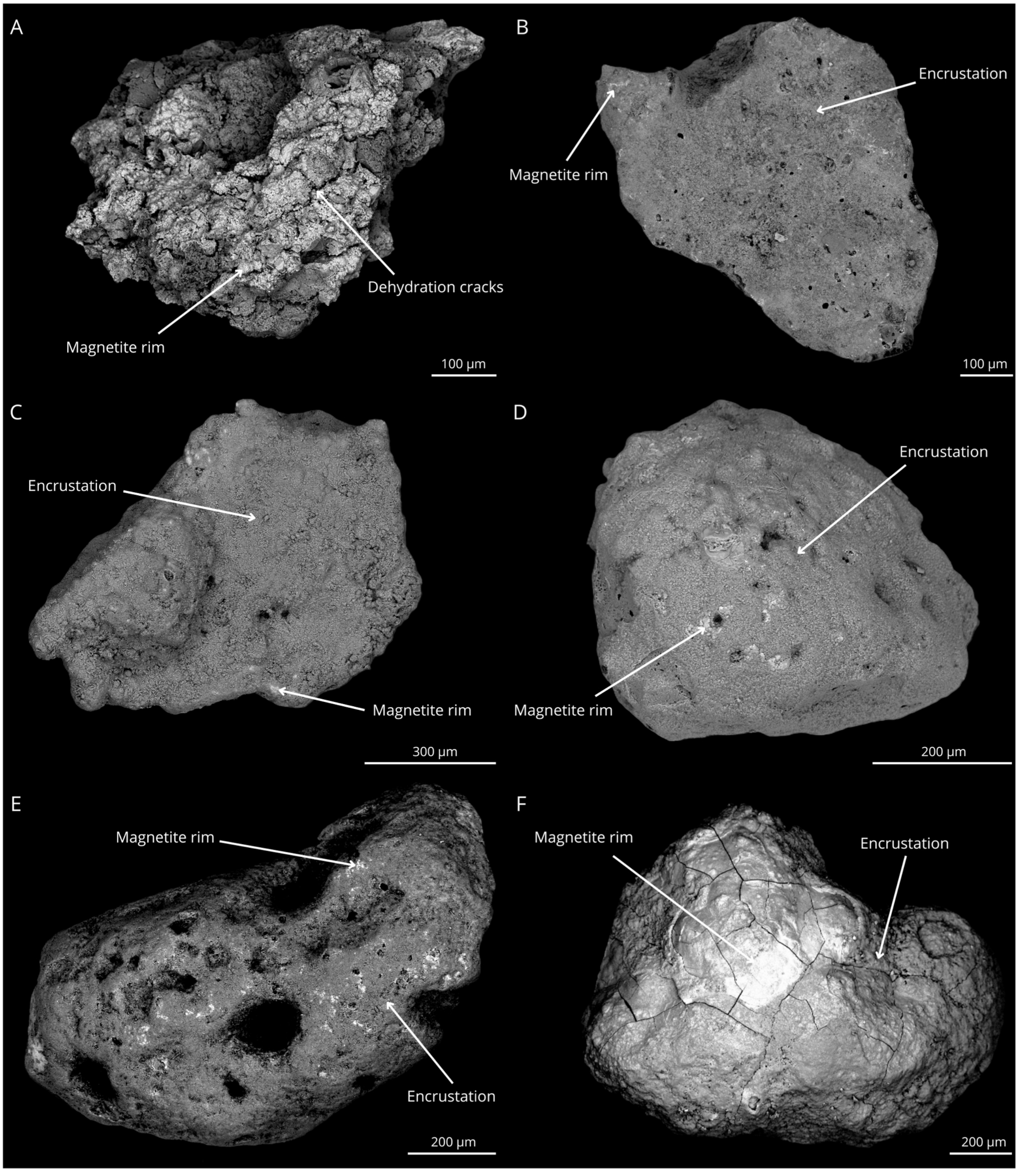


**Figure 2.** Backscattered electron images of the external surface of representative micrometeorites from the Transantarctic Mountains. (a) Angular, fine-grained unmelted micrometeorite (PDT7-5); (b) Angular, coarse-grained unmelted micrometeorite (MIB45-37); (c) Sub-angular, fine-grained scoriaceous micrometeorite (MIB45-14); (d) Sub-rounded, coarse-grained scoriaceous micrometeorite (KIL47-1); (e) Sub-rounded, composite scoriaceous micrometeorite (KIL48-1); (f) Sub-rounded, coarse-grained unmelted micrometeorite (MIB45-73).

angle of 360° with 5 to 8 averaged frames/projection. The projections were reconstructed using the X-Act software (RX Solutions, France). The same software was used for the phase retrieval of the acquired projections prior to reconstruction (Paganin's algorithm; Paganin et al., 2002) and to correct or remove CT artifacts.

10.1029/2026JE009650

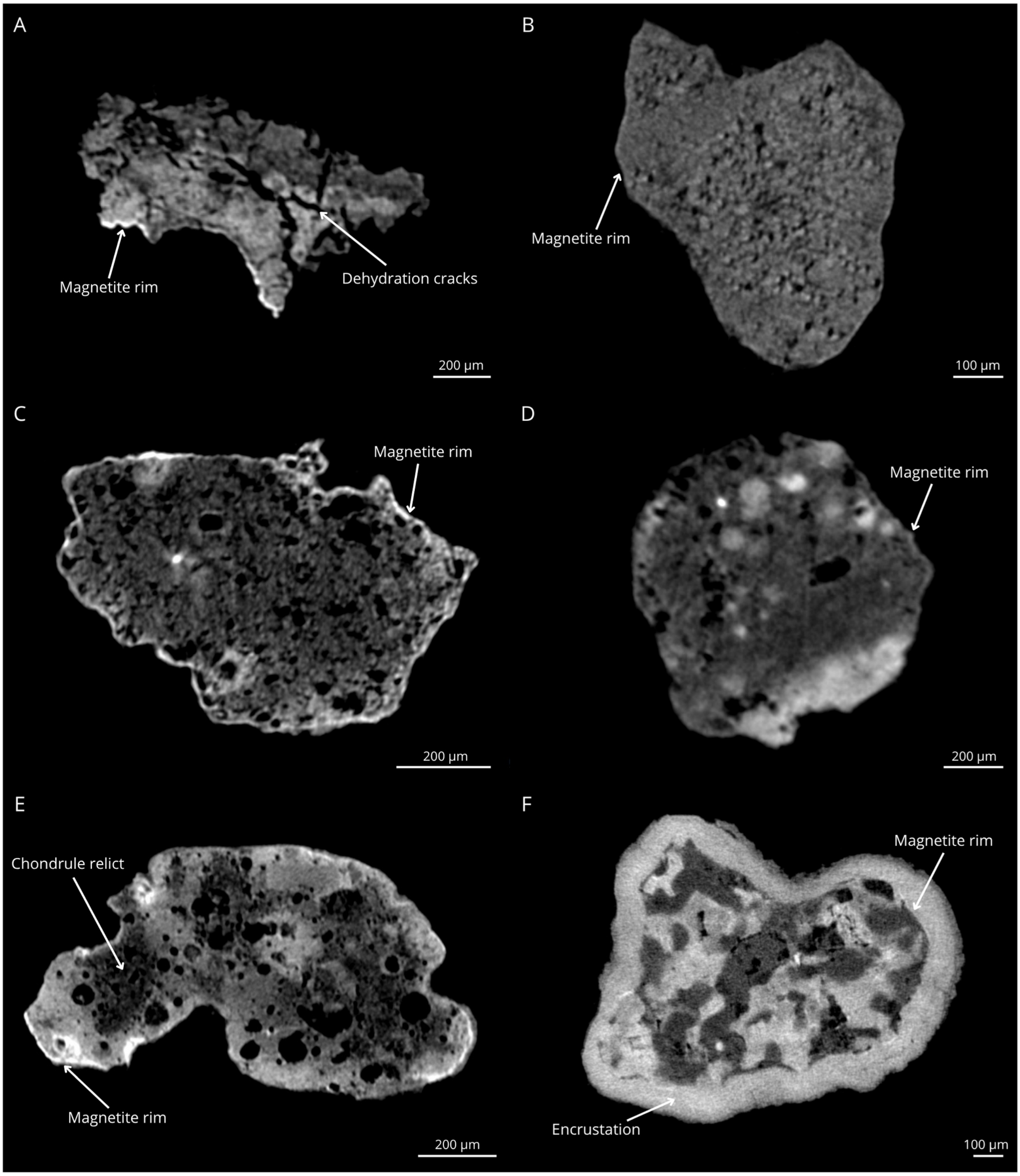


**Figure 3.** Virtual sections obtained by X-ray computed microtomography of representative micrometeorites from the Transantarctic Mountains. (a) Angular, fine-grained unmelted micrometeorite (PDT7-5); (b) Angular, coarse-grained unmelted micrometeorite (MIB45-37); (c) Sub-angular, fine-grained scoriaceous micrometeorite (MIB45-14); (d) Sub-rounded, coarse-grained scoriaceous micrometeorite (KIL47-1); (e) Sub-rounded, composite scoriaceous micrometeorite (KIL48-1); (f) Sub-rounded, heavily weathered, coarse-grained unmelted micrometeorite (MIB45-73).

The visualization of the reconstructed data was obtained using the commercial software Dragonfly 3D World (Version 2024.1, Comet Technologies, Canada).

The classification of micrometeorites was based on the application of textural criteria across both BSE images and μXCT data, including particle morphology, degree of vesiculation, presence and continuity of magnetite or igneous rims, occurrence of dehydration cracks and extent of textural reorganization of primary mineral phases. These criteria were applied systematically across the data set by independent assessments by multiple authors (SO, LF, and MS) and subsequently harmonized through consensus. Although no strict quantitative thresholds were imposed, the combined use of complementary 2D and 3D imaging allows a robust and internally consistent classification. To confirm our textural classification, 22 particles, representative of the range of textures observed in our study population, were embedded in resin, sectioned, and examined using BSE 2D imaging (Figure 4). These images were obtained using a ZEISS Crossbeam 550 FIB-SEM (focused ion beam - scanning electron microscope), equipped with Bruker's QUANTAX EBSD/EDS analysis system for phase identification, at CISUP. The comparison between μXCT data and corresponding polished sections shows good agreement and confirms that the main textural features used for classification can be reliably identified at the achieved voxel resolution. All data generated and analysed during this study, including BSE images of external surfaces, μXCT virtual sections, BSE images of polished sections, and the Excel data set, are openly available via Zenodo (Ottaviani, 2026): https://doi.org/10.5281/zenodo.20184378.

## 3. Results

The sizes reported in this work are spherical equivalent diameters. These were calculated using the formula $\sqrt[3]{a \times b^2}$ (Suavet et al., 2009) where *a* and *b* are the length of the particle's long and short axes, respectively. We determined axis lengths using backscattered (BSE) and secondary electron images of the whole particles.

### 3.1. Identification and Classification of Micrometeorites

Using BSE 2D imaging of the external surface and 3D μXCT sections, the 207 unmelted and scoriaceous micrometeorites were classified according to their petrographic and textural characteristics (Table 1). The distinction between fine-grained and coarse-grained particles (i.e., those with a grain size greater than 1 μm) is determined by the size of the crystals following Genge et al. (2008). Instead, composite micrometeorites consist of coarse-grained igneous objects, commonly interpreted as chondrule fragments, set in a fine-grained matrix (Genge et al., 2005). Ninety-two are unmelted micrometeorites, comprising 35 fine-grained (38%), 53 coarse-grained (58%) and 4 composite (4%) micrometeorites. The remaining 115 are scoriaceous micrometeorites, of which 92 are fine-grained (80%), 10 are coarse-grained (9%) and 13 are composite (11%) micrometeorites.

The micrometeorites studied in this work present a range of irregular shapes, with angular to sub-rounded morphologies (Figure 2). Unmelted micrometeorites are characterised by irregular and angular shapes. They are usually wrapped by a well-defined magnetite rim with few exposed vesicles at the particle surface. By contrast, scoriaceous micrometeorites exhibit sub-rounded shapes and scoriaceous texture. Their surface is mantled by a magnetite rim. In section, scoriaceous particles bear further evidence of partial melting, for example showing an igneous rim (i.e., a surface thin melt layer that crystallized during atmospheric entry; Genge, 2006), a vesicular glassy matrix, and partial textural reorganization of primary mineral grains (Figures 3 and 4).

Chondrules in unmelted micrometeorites may be preserved as intact components, fragmented, or mildly altered, whereas in scoriaceous micrometeorites chondrules are generally partly melted, resorbed and incorporated into a glassy, vesicular matrix. Opaque phases (Fe-metal and Fe-sulphides) commonly undergo thermal decomposition, melting and/or oxidation during atmospheric entry but remain recognizable in some samples. In almost all the samples, the presence of magnetite $\left(Fe^{2+}Fe^{3+}_2O_4\right)$ rim has been identified, consistent with earlier observations that such a rim is characteristic of pulse-heated Fe-bearing silicate minerals during entry into the atmosphere (Folco & Cordier, 2015; Genge et al., 2008; Toppani et al., 2001; Toppani & Libourel, 2003). In most of the studied micrometeorites, the magnetite rim appears as a continuous shell covering the whole particles, while in other specimens the magnetite rim is discontinuous, indicating some fragmentation either at Earth's surface or during atmospheric entry. Dehydration cracks and pipes due to degassing during atmospheric entry heating are observed in some unmelted specimens (Figure 2c). The external surfaces on most of the TAM micrometeorites are affected by terrestrial weathering, with patches or encrustations of jarosite and/or other Ca-bearing salts – common weathering minerals in the TAM collection (Rochette et al., 2008; van Ginneken et al., 2016). In accordance with van Ginneken et al. (2016), the formation of jarosite is contingent upon the specific environmental conditions that prevailed during the process of terrestrial weathering. The prolonged exposure to the

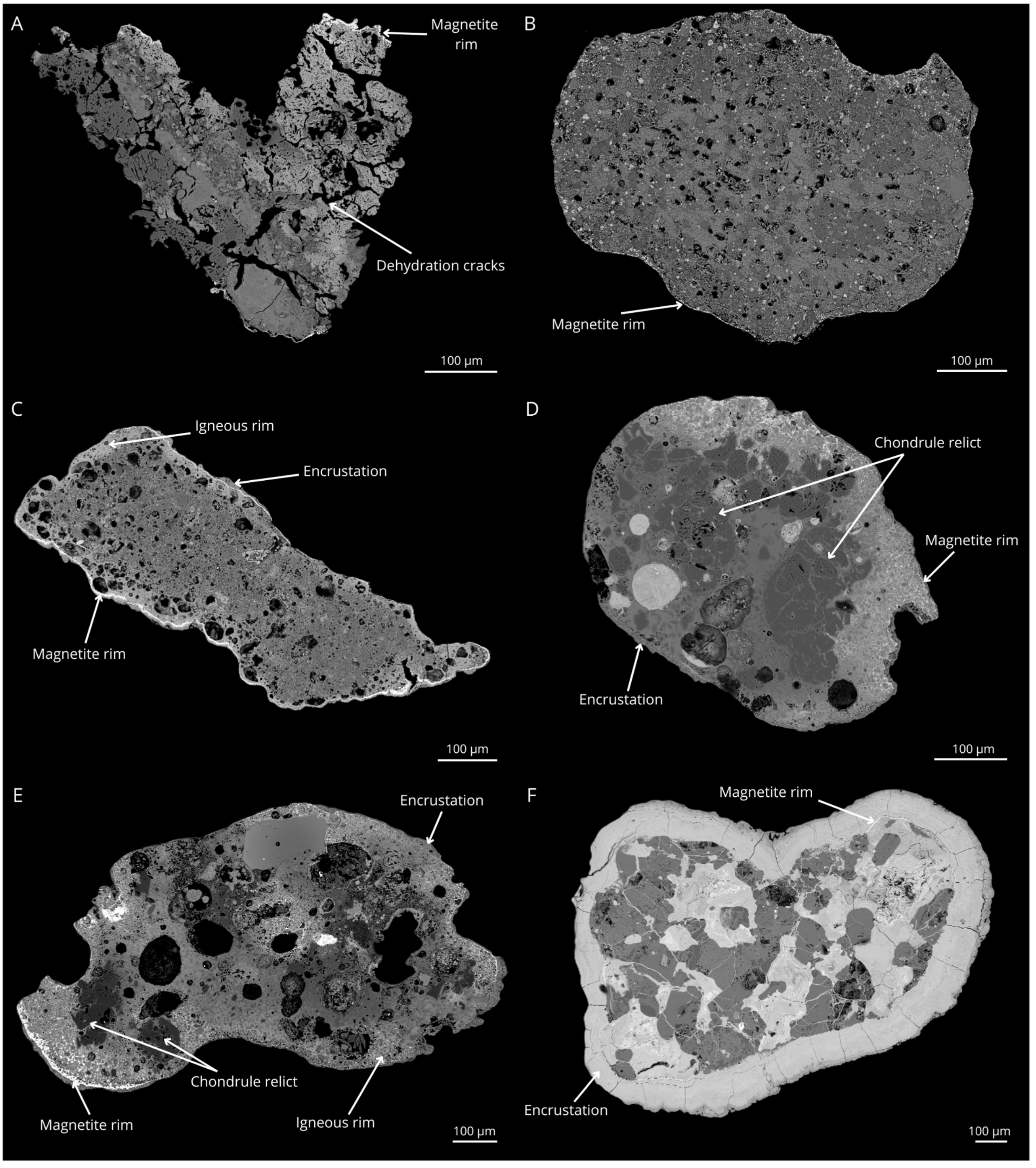


**Figure 4.** Backscattered electron images of polished sectioned representative micrometeorites from the Transantarctic Mountains. (a) Angular, fine-grained unmelted micrometeorite (PDT7-5); (b) Angular, coarse-grained unmelted micrometeorite (MIB45-37); (c) Sub-angular, fine-grained scoriaceous micrometeorite (MIB45-14); (d) Sub-rounded, coarse-grained scoriaceous micrometeorite (KIL47-1); (e) Sub-rounded, composite scoriaceous micrometeorite (KIL48-1); (f) Sub-rounded, heavily weathered, coarse-grained unmelted micrometeorite (MIB45-73).

Antarctic environment resulted in the leaching and dissolution of soluble phases, the alteration of glass and the formation of secondary minerals.

Through the observation of 3D µXCT sections, and based on textures, inferred mineralogy and size, we identified the presence of whole intact and minimally altered chondrules in 29 micrometeorites (∼14% of the population), meaning they can be definitively considered chondritic (e.g., Figure 5). Of these, 15 are composite

10.1029/2026JE009650

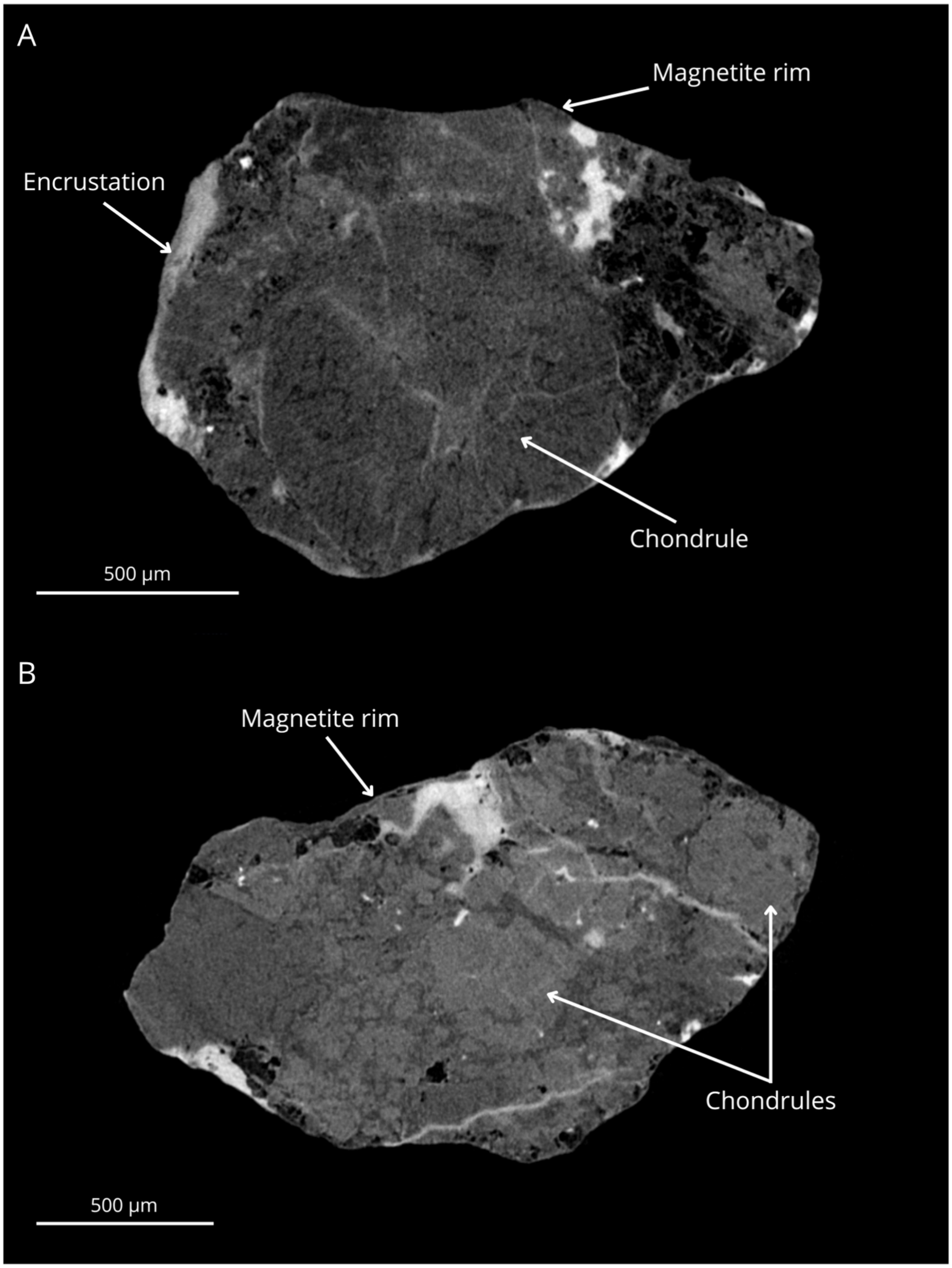


**Figure 5.** X-ray computed microtomography virtual sections of representative examples of chondrule-bearing coarse-grained unmelted micrometeorites from the Transantarctic Mountains. (a) MIB45-65; (b) MIB45-9.

micrometeorites, while 14 are coarse-grained. The percentage of chondrule-bearing particles in different size ranges shows that 38% ($N = 11$) fall into the <500 μm fraction, 34% ($N = 10$) into the 500–1,000 μm range, and 28% ($N = 8$) into the >1,000 μm fraction. When evaluated in relation to the total number of unmelted and scoriaceous micrometeorites in the collection within each size range, the proportion of chondrule-bearing particles increases markedly with size: 9% of particles measuring <500 μm have a chondrule, compared to 14% in the 500–1000 μm range and up to 67% in the >1000 μm range.

In addition to the micrometeorites described above, a subset of particles ($N = 18$) was identified as fragments of larger bodies. These particles are interpreted as disaggregated fragments, likely produced by fragmentation of

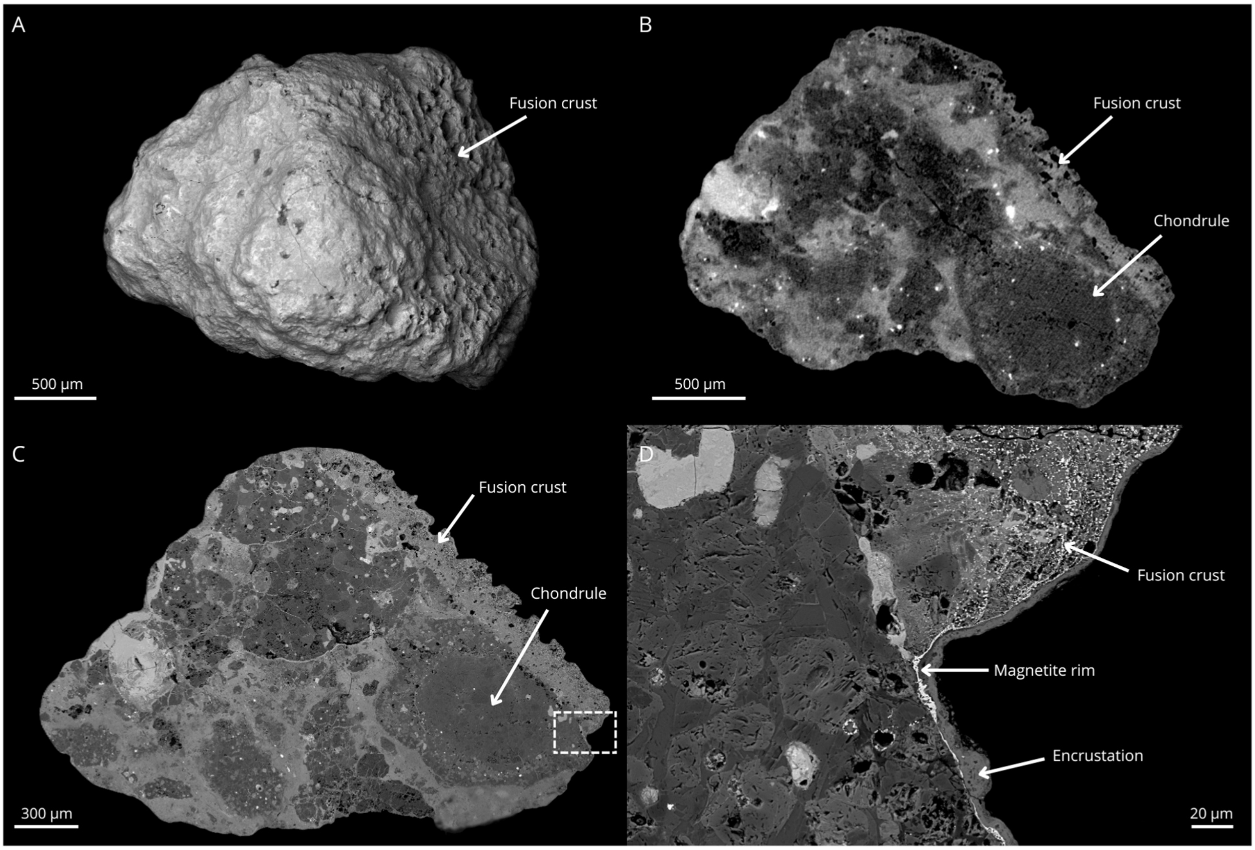


**Figure 6.** An example of a fragmented particle (MIB45-55) identified within the studied Transantarctic Mountains micrometeorite collection. Part of its external surface is covered by fusion crust, part by a magnetite rim as evidence of fragmentation during atmospheric ablative flight. (a) Backscattered electron image of the external surface; (b) Virtual section obtained by X-ray computed microtomography; (c) Backscattered electron image of polished section; white rectangle outlines the region featured in "D." (d) Backscattered electron close-up image of the textural relationship between fusion crust and magnetite rim.

larger meteoroids during atmospheric entry (e.g., Figure 6) or by the mechanical breakup of meteorites after they arrived on Earth. These particles are characterised by irregular morphologies and, in some cases, the presence of a fusion crust restricted to one side, distinguishing them from typical micrometeorites (e.g., Nava et al., 2020). Their sizes range from approximately 400 to 2,900 µm. As incomplete fragments that do not represent whole particles, they were excluded from all statistical analyses presented in this study.

### 3.2. Deviation From Ideal Elliptical Geometry in Unmelted Micrometeorites

To quantify the deviation of the shapes of the unmelted micrometeorites ($N = 92$) from ideal elliptical geometry, we calculated the eccentricity ($e$) of the equivalent ellipse defined by the measured major ($a$) and minor axes ($b$) through SEM imaging, using the formula $e = \sqrt{1 - (b/a)^2}$. Eccentricity is a direct geometric measure of deviation from circularity, and the analysis of our unmelted particles revealed a median eccentricity of 0.62 (IQR 0.43–0.72).

### 3.3. Equivalent Spherical Diameter Versus Mass Relationship

The studied micrometeorite collection ($N = 207$) has equivalent spherical diameters ranging from approximately 170 to 1,650 µm (average diameter ≈515 µm), corresponding to masses ranging from approximately 10 to 4,200 µg (average mass ≈245 µg). The relationship between average particle diameter and mass across the full data set is well-described by a power-law function (Figure 7a):

$$m = 1.07 \times 10^{-6}\, d^{2.96} \tag{1}$$

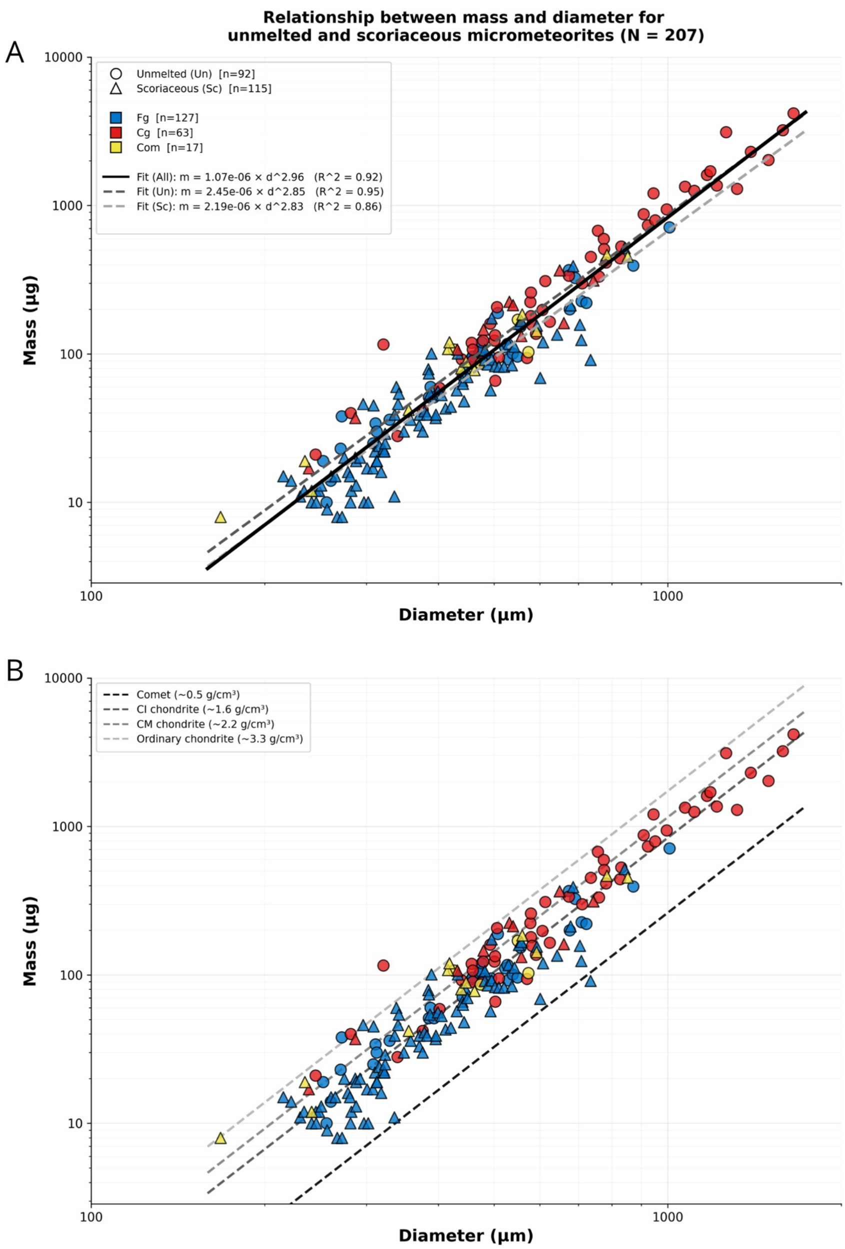


**Figure 7.** Log-log plot showing the relationship between equivalent spherical diameter and mass for unmelted and scoriaceous micrometeorites analysed in this study. (a) Power-law regressions for the entire data set, as well as for unmelted and scoriaceous micrometeorites separately, reveal a strong positive correlation between size and mass, with coefficients of determination ($R^2$) of 0.92, 0.95 and 0.86, respectively. (b) Comparison of the data with meteorite reference density curves (based on Consolmagno et al., 2008) indicates that most micrometeorites fall within a bulk density range of ~1–3 g/cm$^3$, overlapping with carbonaceous chondrites (CI-CM) and remaining lower than ordinary chondrites, but significantly higher than typical cometary materials. Fine-grained (Fg) particles are shown in blue, coarse-grained (Cg) in red, and composite (Com) in yellow.

Where $m$ is mass (μg) and $d$ is equivalent spherical diameter (μm). This fit yields a coefficient of determination of $R^2 = 0.92$. Separate power-law regressions were also calculated for unmelted and scoriaceous micrometeorites (Figure 7a). The unmelted particles follow the power-law function:

$$m = 2.45 \times 10^{-6}\, d^{2.85} \tag{2}$$

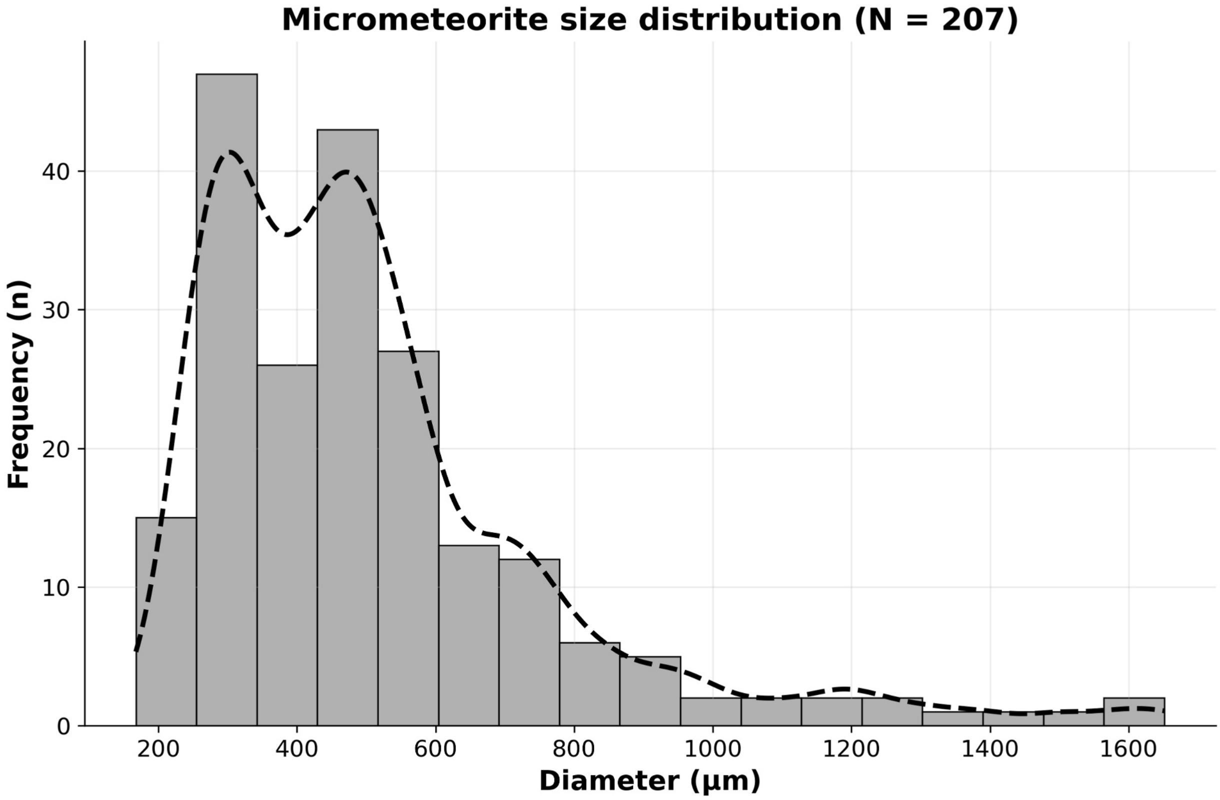


**Figure 8.** The histogram shows the size-frequency distribution of unmelted and scoriaceous micrometeorites as a function of micrometeorite diameter. A Gaussian kernel density estimate is overlaid in black dashed lines, providing an estimation of the sampled continuous distribution. The size-frequency distribution of the collection is visualized with 90 μm bin intervals (Freedman–Diaconis rule), with two peaks present centred at 305 μm and 470 μm.

This fit yields a coefficient of determination of $R^2 = 0.95$. While the scoriaceous micrometeorites are well-described by:

$$m = 2.19 \times 10^{-6}\, d^{2.83} \tag{3}$$

This fit yields a coefficient of determination of $R^2 = 0.86$.

### 3.4. Size-Frequency Distribution

The size-frequency distribution of the TAM micrometeorite population studied in this work can be evaluated using histogram plots (Figures 8 and 9). On considering the entire population (unmelted and scoriaceous, fine-grained and coarse-grained; Figure 8), a pronounced right-skewed distribution with a rapid decline in particle frequency as diameter increases above 1,000 μm is observed. Furthermore, statistical testing (Shapiro–Wilk test [$p$-value = $5.5 \times 10^{-14}$] and the Anderson-Darling test [statistic = 8.417, relative to the 1% critical value 1.072]) rejects a null hypothesis of normality, indicating strong deviation from a normal distribution (Anderson & Darling, 1954; Shapiro & Wilk, 1965). Two local maxima are evident, centred at approximately 305 μm and 470 μm, respectively, thus demonstrating the existence of a bimodal trend in the distribution. This interpretation is supported by kernel density estimation (KDE; Figure 8). A two-component Gaussian Mixture Model (McLachlan & Peel, 2000) fitted to the log-transformed diameters is slightly favoured by the Akaike Information Criterion, although not by the Bayesian Information Criterion. Overall, these results are consistent with a bimodal structure.

The Freedman–Diaconis rule was applied to determine the bin size in the histograms (Figures 8 and 9), as this provides a balanced representation of the data without oversimplifying the distribution or losing detail. This method utilizes the interquartile range, making it less sensitive to outliers and better suited to skewed distributions (Freedman & Diaconis, 1981), as we observe in our data set. To assess the sensitivity of the observed distribution

10.1029/2026JE009650

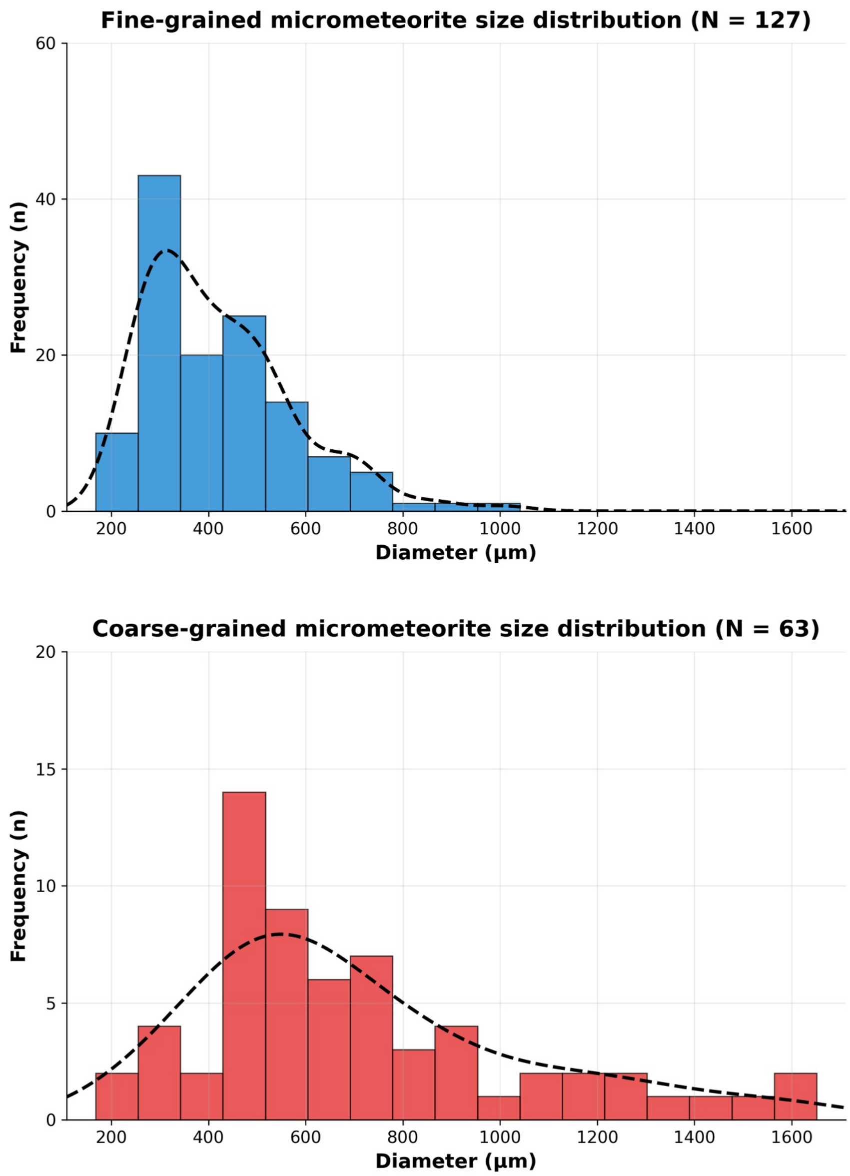


**Figure 9.** The histograms show the size-frequency distribution for the fine-grained (Blue histogram) and coarse-grained (Red histogram) micrometeorites as a function of micrometeorite diameter. The distribution is visualized with a 90 μm bin intervals (Freedman–Diaconis rule) and are overlaid by a Gaussian kernel density estimate (KDE, shown in black dashed lines). The size-frequency distribution of the fine-grained particles show a peak at approximately 315 μm, while the size-frequency distribution of the coarse-grained particles show a peak at approximately 550 μm.

to binning choices, additional histograms were generated using a range of bin widths (Figure S1 in Supporting Information S1). These show that the overall bimodal structure identified by the kernel density estimate is robust across different histogram binning choices.

The size-frequency distribution of the fine- and coarse-grained micrometeorites exhibits a pronounced right-skewed distribution (Figure 9). A comparison of the histogram plots reveals the presence of two distinct peaks in the collection, centred at approximately 315 μm and 550 μm for fine-grained and coarse-grained micrometeorites, respectively. Moreover, in the size-frequency distribution of fine-grained micrometeorites, there are no particles with diameters greater than ∼1 mm. Composite micrometeorites show a peak of particle sizes at approximately 460 μm. However, the number of analysed particles in this group is limited ($N = 17$), preventing a robust statistical treatment.

## 4. Discussion

### 4.1. An Empirical Size-Mass Relation for Micrometeorites

A power-law relationship between micrometeorite mass and diameter (Equation 1 and Figure 7a) is appropriate because mass increases with the cube of diameter, assuming a constant density. Despite heterogeneity arising from variations in micrometeorite density associated with differences in composition (e.g., coarse- vs fine-grained textures) and thermal alteration during atmospheric entry (unmelted vs scoriaceous), the best-fit relationship provides a robust empirical description of the overall population, integrating particles that have experienced different degrees of atmospheric processing ($R^2 = 0.92$). This empirically defined relationship provides a practical means of rapidly estimating particle mass, which may prove useful in future studies. Spherical equivalent diameter can be measured rapidly and accurately under SEM, whereas direct measurement of particle mass requires specialised equipment and repeated micromanipulation of each particle. The relationship may also prove valuable for numerical models aiming to constrain the mass flux of cosmic dust accreted by Earth across a wide range of particle sizes.

The relationship between mass and diameter provides a first-order constraint on the bulk density of the studied micrometeorites. However, it is important to note that the regression derived from the full data set combines unmelted and scoriaceous particles, which record different degrees of atmospheric processing. Unmelted micrometeorites more closely preserve their primary densities, whereas scoriaceous particles have experienced partial melting, vesiculation, and internal reorganisation during atmospheric entry, resulting in increased porosity and reduced bulk density (e.g., Genge, 2017a).

The micrometeorites of this study typically have bulk densities between 1,000 and 3,000 kg $m^{-3}$ (Figure 7b). Interestingly, micrometeorite densities are lower than those of ordinary chondrites, which have reported bulk densities of approximately 3,300 kg $m^{-3}$. Instead, the micrometeorite population overlap with the density of CM chondrites and CI chondrites, which have reported bulk densities of approximately 2,200 and 1,600 kg $m^{-3}$, respectively (Consolmagno et al., 2008). However, they remain substantially higher than bulk densities estimated for cometary nuclei, which are typically $\ll$1,000 kg $m^{-3}$ (e.g., Consolmagno et al., 2008; Davidsson & Gutiérrez, 2004). Particles plotting closer to the lower-density curves are predominantly scoriaceous fine-grained, consistent with enhanced internal porosity produced during atmospheric entry. These first-order density estimates for the studied micrometeorites are based on simplified assumptions of particle equivalent spherical diameters and do not explicitly account for irregular shapes, elevated particle eccentricities (Section 3.2), internal porosity, or possible terrestrial alteration (e.g. oxidation of metallic phases). In addition, the bulk densities reported for ordinary and carbonaceous chondrites are generally measured on substantially larger samples and therefore incorporate larger-scale porosity structures that are not represented within the much smaller micrometeorite volumes analysed here. Moreover, the use of spherical equivalent diameters provides a standardized geometric approximation suitable for consistent statistical comparison across the studied population. The resulting density estimates should therefore be regarded as first-order approximations.

### 4.2. Comparison of Size-Frequency Distribution in the TAM Collection

The identification of two distinct peaks at approximately 305 μm and 470 μm suggests that the large TAM scoriaceous and unmelted micrometeorite population is bimodal, with two subpopulations (Figure 8). A similar bimodal size distribution was observed in the TAM cosmic spherules (TAM65 collection; $n = 1,643$; size range: 100 to 2,000 μm), yet shifted towards lower sizes with the most common micrometeorite size peaking at approximately 250 μm and a minor peak at approximately 145 μm (Suttle & Folco, 2020). This cosmic spherule size distribution is consistent with data from other Antarctic micrometeorite collections, wherein the vast majority of particles were cosmic spherules. In the Larkman Nunatak, the cosmic spherule size distribution peak was reported to be 210–330 μm (Genge et al., 2018), while in the South Pole Water Well collection it is at 200–250 μm (Taylor et al., 1998, 2000).

The shift of the peaks in cosmic spherules versus unmelted-scoriaceous micrometeorite size distributions can be explained in the context of atmospheric entry conditions studied by Love and Brownlee (1991), Taylor et al. (1998), Rudraswami et al. (2012), Briani et al. (2013) and Genge (2016), Genge (2017b). Upon atmospheric entry, extraterrestrial dust undergoes aerodynamic heating due to atmospheric deceleration from cosmic velocities (>12 km/s) and thus variable mass loss according to variable extents of evaporation, ablation and, to a lesser

10.1029/2026JE009650

extent fragmentation (e.g., Rudraswami et al., 2012; Suttle, Genge, et al., 2019). These processes contribute to a decrease in the average size-mass of melted micrometeorites, thereby increasing the abundance of smaller particles. The collection of TAM scoriaceous and unmelted micrometeorites presented in this study was derived from particles recovered from several TAM micrometeorite traps and selected by investigating sediments with homogeneous grain-size obtained from the sieving process. Therefore, the collection of scoriaceous and unmelted micrometeorites can be considered as an overall average in the TAM collection for these types of cosmic dust. Scoriaceous and unmelted micrometeorites are generally more fragile and more challenging to preserve and identify than cosmic spherules. Nevertheless, their recovery from multiple TAM micrometeorite traps and across different size fractions suggests that the studied collection captures a broad range of the unmelted and partially melted micrometeorite population present within the TAM deposits. The observed discrepancy between the bimodal size-frequency distribution of scoriaceous and unmelted micrometeorites and that of cosmic spherules (Suttle & Folco, 2020) is therefore unlikely to result solely from sampling bias and can be plausibly explained by the size-mass reduction produced by atmospheric entry heating acting on a single population of extraterrestrial dust.

### 4.3. Global Mass Flux Over the Quaternary

We have identified an average mass loss of 87% in the flux of interplanetary dust particles undergoing complete melting during atmospheric entry heating. It should be noted that the reference population used in this comparison includes both unmelted and scoriaceous micrometeorites, which represent different stages of atmospheric processing. Therefore, the estimated mass loss should be interpreted as a first-order approximation of the transition from partially processed particles to fully melted cosmic spherules, rather than a direct measure of mass loss from pristine precursor material. This mass loss estimate is based on the percentage difference between the masses corresponding to the peaks identified in the size-frequency distributions of our collection (at diameters of 305 μm and 470 μm, corresponding to 24 μg and 87 μg, according to Equation 1) and the TAM cosmic spherule collection (Suttle & Folco, 2020; at diameters of 145 μm and 250 μm, corresponding to 3 μg and 13 μg, according to Equation 1). Specifically, we compared the mass of the first peak in each collection and did the same for the second peak. The two resulting percentage differences, 89% and 85%, respectively, were then averaged to yield the mean percentage mass loss of 87%. This value is fully consistent with values reported in previous modelling and experimental studies of micrometeorite atmospheric processing. According to Love and Brownlee (1991), at least 90% of the mass in silicate-dominated (S-type) micrometeoroids with a diameter of approximately 100–1000 μm evaporates during atmospheric entry. The same percentage of evaporation during atmospheric ingress was reported in Taylor et al. (1998). As stated in their study, this estimate was deduced by comparing micrometeoroid influx measured using the NASA Long Duration Exposure Facility (LDEF) satellite (Love & Brownlee, 1993) with the flux of surviving melted particles (namely, cosmic spherules in the 50–700 μm size range) collected from the bottom of the South Pole Water Well. Moreover, simulations conducted by Briani et al. (2013) demonstrate that the processes of melting, sputtering, and evaporation contribute to a mass loss of up to approximately 80% in melted micrometeorites (assuming a density of 3 g/cm$^3$, an entry angle of 45° and an entry speed of 11.2 km/s).

The estimated average mass loss of 87% provides the opportunity to convert the earlier micrometeorite mass flux at Earth's surface of 1,555 (±753) t/yr estimated by Suttle and Folco (2020) from the TAM cosmic spherules collection, into the global flux of interplanetary dust entering Earth's atmosphere. The estimate of the micrometeorite mass flux at Earth's surface by Suttle and Folco (2020) is based upon a collection area of 0.5 m$^2$, an accumulation window between 0.8 and 2.3 Ma and a total mass of 1.772 g for the entire micrometeorite budget within the TAM65 trap at Miller Butte. As discussed in that study, this estimate is subject to uncertainties, particularly related to the duration of the accumulation window and the exact surface area sampled by the micrometeorite trap. Based on the 87% mass-loss during atmospheric entry, we derive a first-order, time-averaged mass flux of cosmic dust (within the 100–2,000 μm size range) that reaches the Earth's atmosphere over the Quaternary period of ∼12,000 (±6,000) t/yr or ∼32 t/d. This estimate should be considered as an order-of-magnitude approximation and is contingent upon the same caveats as those outlined by Suttle and Folco (2020).

In consideration of our specified fall time window and particle size range, the estimated pre-atmospheric flux is broadly comparable to previous measurements and models of cosmic dust accretion at Earth. Love and Brownlee (1993) estimated a terrestrial dust accretion rate of 40,000 ± 20,000 t/yr from crater-counting surveys of the NASA LDEF. However, a later recalculation by Cremonese et al. (2012), using revised crater radius-to-mass relationships, suggested lower values of 7,400 ± 1,000 t/yr for asteroidal dust (and 4,200 t/yr for cometary dust), with a mass peak at approximately 100 μm diameter. Moreover, our estimate of the total dust mass input before atmospheric entry is consistent with those obtained by combining a Chemical Ablation Model with a Zodiacal Cloud Model (ZoDy) presented in previous studies by Carrillo-Sánchez et al. (2020) and Rojas et al. (2021), yielding 10,220 ± 5,840 t/yr and ∼15,000 t/yr, respectively. Overall, the broad compatibility between LDEF-derived estimates, modern ablation models and the Quaternary flux reconstructed from Antarctic micrometeorite traps (Suttle & Folco, 2020) suggests that Earth has received a relatively stable input of large micrometeorites over the last few million years.

### 4.4. Bimodal Size-Frequency Distribution in the Micrometeorite Flux and Implications for End-Member Materials

The bimodal size-frequency distribution observed in the unmelted-scoriaceous and melted micrometeorite flux (this study and Suttle & Folco, 2020, respectively) is best interpreted as reflecting the contribution of two end-member material populations with contrasting mechanical properties within the near-Earth interplanetary dust complex. These are hydrous, matrix-rich fine-grained chondritic materials and anhydrous (or nearly so), chondrule-bearing and coarse-grained chondritic or achondritic materials, which broadly relate to primitive and more evolved reservoirs, respectively (Cordier & Folco, 2014; Fernandes et al., 2025; Suavet et al., 2010; van Ginneken et al., 2017).

Fine-grained micrometeorites are distinguished by an amorphous groundmass with embedded microcrystals and a prevalence of hydrated and organic phases (Dobrică et al., 2011; Genge et al., 1997, 2008; Kurat et al., 1994; Suttle, Folco, et al., 2019; Suttle, Genge, & Russell, 2017). Based on mineralogical, isotopic, and spectroscopic evidence, these fine-grained micrometeorites show strong affinities with primitive hydrated carbonaceous precursors (CI/CM/CR and C2-ungrouped chondrites) and, to a lesser extent, with cometary material. These features suggest a parentage with C-type asteroids or cometary sources (Cordier & Folco, 2014; Dobrică et al., 2011; Fernandes et al., 2025; Genge et al., 1997, 2008; Kurat et al., 1994; Nava et al., 2020; Suttle, Folco, et al., 2019; Suttle, Genge, & Russell 2017; Suttle et al., 2020; Van Maldeghem et al., 2023). Coarse-grained micrometeorites are characterised by the prevalence of coarse-grained, anhydrous (or nearly so) silicate assemblages. Their textures and compositions are consistent with chondrule materials, primarily isolated or fragmented chondrules from type 3 chondrites, or with recrystallized chondritic materials from equilibrated chondrites associated with C- or S-type asteroids, respectively (Cordier et al., 2018; Fernandes et al., 2025; Folco & Cordier, 2015; Genge, 2008a, 2008b; Genge et al., 2005, 2008; van Ginneken et al., 2012; Van Maldeghem et al., 2023). Furthermore, a small fraction of coarse-grained melted and unmelted micrometeorites has been linked to evolved achondritic parent bodies (Badjukov et al., 2010; Brase et al., 2021; Cordier et al., 2012; Genge, 2017b; Gounelle et al., 2009; Soens et al., 2022). Composite micrometeorites are most consistent with carbonaceous chondrite materials, in which abundant hydrated matrix and anhydrous components (e.g., chondrules) coexist at the submillimetre to millimetre scale. Their occurrence demonstrates that fine- and coarse-grained micrometeorites do not necessarily derive from distinct parent bodies, but can instead represent fragments of the same chondritic parent body sampling different proportions of chondritic components. Taken together, fine-grained and composite micrometeorites predominantly sample carbonaceous, aqueously altered parent bodies (Genge, 2008b; Genge et al., 2005; Suttle, Genge, Folco, & Russell, 2017; Suttle, Folco, et al., 2019; Suttle et al., 2020; Van Maldeghem et al., 2023).

Chondritic fine-grained matrix materials on one side and coarse-grained chondrules or equilibrated chondritic and achondritic materials on the other have distinct mechanical strengths, which strongly influence fragmentation behaviour in space and survivability during atmospheric entry (Cordier & Folco, 2014; Genge et al., 1997, 2008; Suavet et al., 2010; van Ginneken et al., 2017, 2024). Fine-grained micrometeorites, which are rich in phyllosilicates and analogous to the matrices of carbonaceous chondrites, have friable and porous textures that favour the production of fine dust upon collisional disruption of their parent materials in space (Flynn et al., 2009; Suavet et al., 2010). By contrast, coarse-grained micrometeorites, dominated by mechanically robust dry or weakly hydrated minerals, show enhanced resistance to fragmentation and are therefore more likely to survive as larger particles (Genge et al., 1997, 2008, 2020; Suttle, Genge, & Russell, 2017; Taylor et al., 2012; Van Maldeghem et al., 2023).

The bimodality in the size-frequency distribution of the fine- and coarse-grained micrometeorites observed in this study (Figures 8 and 9), with a fine-grained cluster well-separated from a coarse-grained cluster, can thus be explained through a dust production mechanism in space mainly through collisions of chondritic parent bodies.

This process preferentially generates smaller micrometeoroids from fine-grained precursor materials and larger micrometeoroids from coarse-grained precursor materials. The size-frequency distribution of the fine-grained micrometeorites also shows a sharp decline for sizes over 1 mm. This is also consistent with the expected size distribution of the dust production from the hydrated, matrix-rich chondrites when they are catastrophically disrupted, as observed in experiments conducted by Flynn et al. (2009).

The fine- versus coarse-grained bimodality observed in the present study is a recurring feature in various Antarctic micrometeorite collections. Indeed, fine-grained micrometeorites generally show a smaller range of sizes in comparison to coarse-grained micrometeorites (Genge et al., 2008, 2020; van Ginneken et al., 2024; Van Maldeghem et al., 2023). Taken together, these observations suggest that the bimodality of the size-frequency distribution documented in this study likely reflects the contrasting physical properties of matrix-rich and chondrule-dominated materials, which influence their fragmentation behaviour during dust production in space. Within this framework, fine-grained and coarse-grained micrometeorites represent end-member material populations, while composite micrometeorites provide direct evidence of their coexistence within individual precursor materials.

## 5. Conclusions

We studied a statistically significant number ($N = 207$) of unmelted and scoriaceous micrometeorites from the TAM micrometeorite collection in the approximately 170–1,650 μm size range. The analysis of the size-frequency distribution of these particles demonstrates that this micrometeorite collection is bimodal, with peaks centred at approximately 305 μm and 470 μm. A similar bimodal size-frequency distribution was observed in an earlier study of the TAM cosmic spherule collection, yet shifted towards lower sizes, with peaks centred at approximately 145 μm and 250 μm (Suttle & Folco, 2020). This shift in the bimodal size-frequency distribution of unmelted and scoriaceous micrometeorites versus melted cosmic spherules in the TAM collection is consistent with a first-order average mass loss of approximately 87% in the particles undergoing complete melting during atmospheric entry heating.

The size-frequency distribution of the fine-grained and coarse-grained micrometeorites reflects contrasting lithological end-member components within the interplanetary dust flux. The two distinct size peaks in the scoriaceous plus unmelted micrometeorite collection are centred at approximately 315 μm and 550 μm for fine-grained and coarse-grained micrometeorites, respectively. Fine-grained micrometeorites are dominated by matrix-rich, hydrous materials typical of primitive carbonaceous precursors, whereas coarse-grained micrometeorites are characterised by chondrule-bearing, comparatively dry or less hydrous materials associated with more evolved precursors. These differences are consistent with contrasting mechanical properties that influence fragmentation during dust production in space. Composite micrometeorites represent an intermediate lithological expression, in which fine-grained matrices and coarse-grained igneous components coexist within single particles. Their occurrence supports the interpretation that fine- and coarse-grained micrometeorites do not necessarily derive from strictly separate parent bodies, but may instead represent fragments sampling different lithological domains and proportions of chondritic components within heterogeneous precursor materials.

Based on current mass flux estimates from TAM cosmic spherules (i.e., time- and accumulation-surface-resolved collection) provided by Suttle and Folco (2020), and accounting for the inferred first-order mass loss due to the ablative flight of the micrometeoroid flux, we calculate a time-averaged pre-atmospheric mass flux of ∼12,000 (±6,000) t/yr over the Quaternary period. This result is consistent with current estimates from the LDEF experiment (Love & Brownlee, 1993) and the CABMOD-ZoDy models (Carrillo-Sánchez et al., 2020; Rojas et al., 2021), suggesting that the flux has remained broadly stable over the last few million years.

## Conflict of Interest

The authors declare no conflicts of interest relevant to this study.

## Availability Statement

The complete data set supporting the findings of this study, including the Excel data set, BSE images of external surfaces, μXCT virtual sections, and BSE images of polished sections, is openly available in a Zenodo repository (Ottaviani, 2026): https://doi.org/10.5281/zenodo.20184378.

**Acknowledgments**

The study of TAM micrometeorites at the University of Pisa is supported by the Programma Nazionale di Ricerche in Antartide (PNRA) funded by the Italian MUR, and facilitated by the Space It Up project funded by ASI and MUR (Contract n. 2024-5-E.0 - CUP n. I53D24000060005), as well as by the PRIN 2022 project "Cosmic Dust II: Cosmochemistry and Space Tweezers Technologies for Solar System Science and Exploration", funded by MUR (Project n. 2022S5A2N7 - CUP n. I53D23000730006). Most of this work is part of the MSc thesis of Samuele Ottaviani carried out at the Dipartimento di Scienze della Terra, University of Pisa. This study would not have been possible without the sustained efforts of numerous researchers at the University of Pisa who, over the past two decades, have contributed to the recovery, identification, and curation of the TAM micrometeorite collection. Their work searching sediments under the optical microscope for unmelted and scoriaceous micrometeorites, and the subsequent curation of these materials, laid the foundation for this research. Likewise, we are indebted to previous grants from PNRA that facilitated long-term micrometeorite research. ZAG authors acknowledge the Slovenian node of E-RIHS (I0-E012) and financial support from the Slovenian Research and Innovation Agency (core funding P2-0273, Infrastructure I0-0032, and equipment co-financed under Paket 21 and 23). We thank Matthew Genge and Steven Goderis for thoughtful and constructive reviews, as well as, Debra Buczkowski for editorial handling. Open access publishing facilitated by Universita degli Studi di Perugia, as part of the Wiley - CRUI-CARE agreement.

## References

Anderson, T. W., & Darling, D. A. (1954). A test of goodness-of-fit. *Journal of the American Statistical Association*, *49*(268), 765–769. https://doi.org/10.1080/01621459.1954.10501232

Badjukov, D. D., Brandstaetter, F., Raitala, J., & Kurat, G. (2010). Basaltic micrometeorites from the Novaya Zemlya glacier. *Meteoritics & Planetary Science*, *45*(9), 1502–1512. https://doi.org/10.1111/j.1945-5100.2010.01125.x

Badyukov, D. D., Brandstaetter, F., & Topa, D. (2018). Fine-grained scoriaceous and unmelted micrometeorites: sources and relationships with cosmic spherules. *Geochemistry International*, *56*(11), 1071–1083. https://doi.org/10.1134/S0016702918110022

Brase, L. E., Harvey, R., Folco, L., Suttle, M. D., McIntosh, E. C., Day, J. M., & Corrigan, C. M. (2021). Microtektites and glassy cosmic spherules from new sites in the Transantarctic Mountains, Antarctica. *Meteoritics & Planetary Science*, *56*(4), 829–843. https://doi.org/10.1111/maps.13634

Briani, G., Pace, E., Shore, S. N., Pupillo, G., Passaro, A., & Aiello, S. (2013). Simulations of micrometeoroid interactions with the Earth atmosphere. *Astronomy & Astrophysics*, *552*, A53. https://doi.org/10.1051/0004-6361/201219658

Carrillo-Sánchez, J. D., Gómez-Martín, J. C., Bones, D. L., Nesvorný, D., Pokorný, P., Benna, M., et al. (2020). Cosmic dust fluxes in the atmospheres of Earth, Mars, and Venus. *Icarus*, *335*, 113395. https://doi.org/10.1016/j.icarus.2019.113395

Carrillo-Sánchez, J. D., Nesvorný, D., Pokorný, P., Janches, D., & Plane, J. M. C. (2016). Sources of cosmic dust in the Earth's atmosphere. *Geophysical research letters*, *43*(23), 11–979. https://doi.org/10.1002/2016GL071697

Cassidy, W., Harvey, R., Schutt, J., Delisle, G., & Yanai, K. (1992). The meteorite collection sites of Antarctica. *Meteoritics*, *27*(5), 490–525. https://doi.org/10.1111/j.1945-5100.1992.tb01073.x

Consolmagno, G. J., Britt, D. T., & Macke, R. J. (2008). The significance of meteorite density and porosity. *Geochemistry*, *68*(1), 1–29. https://doi.org/10.1016/j.chemer.2008.01.003

Cordier, C., Baecker, B., Ott, U., Folco, L., & Trieloff, M. (2018). A new type of oxidized and pre-irradiated micrometeorite. *Geochimica et Cosmochimica Acta*, *233*, 135–158. https://doi.org/10.1016/j.gca.2018.04.010

Cordier, C., & Folco, L. (2014). Oxygen isotopes in cosmic spherules and the composition of the near Earth interplanetary dust complex. *Geochimica et Cosmochimica Acta*, *146*, 18–26. https://doi.org/10.1016/j.gca.2014.09.038

Cordier, C., Suavet, C., Folco, L., Rochette, P., & Sonzogni, C. (2012). HED-like cosmic spherules from the Transantarctic Mountains, Antarctica: Major and trace element abundances and oxygen isotopic compositions. *Geochimica et Cosmochimica Acta*, *77*, 515–529. https://doi.org/10.1016/j.gca.2011.10.021

Cordier, C., van Ginneken, M., & Folco, L. (2011). Nickel abundance in stony cosmic spherules: Constraining precursor material and formation mechanisms. *Meteoritics & Planetary Science*, *46*(8), 1110–1132. https://doi.org/10.1111/j.1945-5100.2011.01218.x

Cremonese, G., Borin, P., Martellato, E., Marzari, F., & Bruno, M. (2012). New calibration of the micrometeoroid flux on Earth. *The Astrophysical Journal Letters*, *749*(2), L40. https://doi.org/10.1088/2041-8205/749/2/L40

Davidsson, B. J., & Gutiérrez, P. J. (2004). Estimating the nucleus density of Comet 19P/Borrelly. *Icarus*, *168*(2), 392–408. https://doi.org/10.1016/j.icarus.2003.11.009

Dermott, S. F., Kehoe, T. J., Grogan, K., Durda, D. D., Jayaraman, S., Kortenkamp, S. J., & Wyatt, M. C. (2001). Orbital evolution of interplanetary dust. *Interplanetary dust*, 569–639. https://doi.org/10.1007/978-3-642-56428-4_12

Dionnet, Z., Suttle, M. D., Longobardo, A., Rotundi, A., Folco, L., Della Corte, V., & King, A. (2020). X-ray computed tomography: Morphological and porosity characterization of giant Antarctic micrometeorites. *Meteoritics & Planetary Science*, *55*(7), 1581–1599. https://doi.org/10.1111/maps.13533

Dobrică, E., Engrand, C., Quirico, E., Montagnac, G., & Duprat, J. (2011). Raman characterization of carbonaceous matter in CONCORDIA Antarctic micrometeorites. *Meteoritics & Planetary Science*, *46*(9), 1363–1375. https://doi.org/10.1111/j.1945-5100.2011.01235.x

Fernandes, D., Rudraswami, N. G., & Singh, V. P. (2025). Petrography of scoriaceous and unmelted micrometeorites from the Maitri Station, Antarctica collection. *Advances in Space Research*, *76*(5), 3171–3199. https://doi.org/10.1016/j.asr.2025.06.060

Flynn, G. J. (2001). Atmospheric entry heating of interplanetary dust. In *Accretion of extraterrestrial matter throughout Earth's history* (pp. 107–127). Springer US. https://doi.org/10.1007/978-1-4419-8694-8_7

Flynn, G. J., Durda, D. D., Sandel, L. E., Kreft, J. W., & Strait, M. M. (2009). Dust production from the hypervelocity impact disruption of the Murchison hydrous CM2 meteorite: Implications for the disruption of hydrous asteroids and the production of interplanetary dust. *Planetary and Space Science*, *57*(2), 119–126. https://doi.org/10.1016/j.pss.2008.09.005

Folco, L., & Cordier, C. (2015). Micrometeorites. *EMU Notes in Mineralogy*, *15*(9), 253–297. https://doi.org/10.1180/EMU-notes.15.9

Folco, L., D'Orazio, M., Gemelli, M., & Rochette, P. (2016). Stretching out the Australasian microtektite strewn field in Victoria Land Transantarctic Mountains. *Polar Science*, *10*(2), 147–159. https://doi.org/10.1016/j.polar.2016.02.004

Folco, L., D'Orazio, M., Tiepolo, M., Tonarini, S., Ottolini, L., Perchiazzi, N., et al. (2009). Transantarctic Mountain microtektites: geochemical affinity with Australasian microtektites. *Geochimica et Cosmochimica Acta*, *73*(12), 3694–3722. https://doi.org/10.1016/j.gca.2009.03.021

Folco, L., Rochette, P., Perchiazzi, N., D'Orazio, M., Laurenzi, M. A., & Tiepolo, M. (2008). Microtektites from Victoria land transantarctic mountains. *Geology*, *36*(4), 291–294. https://doi.org/10.1130/G24528A.1

Freedman, D., & Diaconis, P. (1981). On the histogram as a density estimator: L2 theory. *Zeitschrift für Wahrscheinlichkeitstheorie und verwandte Gebiete*, *57*(4), 453–476. https://doi.org/10.1007/BF01025868

Ganovex Team. (1987). Geological map of North Victoria land, Antarctica, 1: 500,000— explanatory notes. *Geologisches Jahrbuch B*, *66*, 7–79.

Genge, M. J. (2006). Igneous rims on micrometeorites. *Geochimica et Cosmochimica Acta*, *70*(10), 2603–2621. https://doi.org/10.1016/j.gca.2006.02.005

Genge, M. J. (2008a). Koronis asteroid dust within Antarctic ice. *Geology*, *36*(9), 687–690. https://doi.org/10.1130/G24493A.1

Genge, M. J. (2008b). Micrometeorites and their implications for meteors. *Earth, Moon, and Planets*, *102*(1), 525–535. https://doi.org/10.1007/s11038-007-9185-z

Genge, M. J. (2016). The origins of I-type spherules and the atmospheric entry of iron micrometeoroids. *Meteoritics & Planetary Science*, *51*(6), 1063–1081. https://doi.org/10.1111/maps.12645

Genge, M. J. (2017a). An increased abundance of micrometeorites on Earth owing to vesicular parachutes. *Geophysical Research Letters*, *44*(4), 1679–1686. https://doi.org/10.1002/2016GL072490

Genge, M. J. (2017b). The entry heating and abundances of basaltic micrometeorites. *Meteoritics & Planetary Science*, *52*(5), 1000–1013. https://doi.org/10.1111/maps.12830

Genge, M. J., Engrand, C., Gounelle, M., & Taylor, S. (2008). The classification of micrometeorites. *Meteoritics & Planetary Science*, *43*(3), 497–515. https://doi.org/10.1111/j.1945-5100.2008.tb00668.x

Genge, M. J., Gileski, A., & Grady, M. M. (2005). Chondrules in Antarctic micrometeorites. *Meteoritics & Planetary Science*, *40*(2), 225–238. https://doi.org/10.1111/j.1945-5100.2005.tb00377.x

Genge, M. J., Grady, M. M., & Hutchison, R. (1997). The textures and compositions of fine-grained Antarctic micrometeorites: Implications for comparisons with meteorites. *Geochimica et Cosmochimica Acta*, *61*(23), 5149–5162. https://doi.org/10.1016/S0016-7037(97)00308-6

Genge, M. J., van Ginneken, M., & Suttle, M. D. (2020). Micrometeorites: insights into the flux, sources and atmospheric entry of extraterrestrial dust at Earth. *Planetary and Space Science*, *187*, 104900. https://doi.org/10.1016/j.pss.2020.104900

Genge, M. J., van Ginneken, M., Suttle, M. D., & Harvey, R. P. (2018). Accumulation mechanisms of micrometeorites in an ancient supraglacial moraine at Larkman Nunatak, Antarctica. *Meteoritics & Planetary Science*, *53*(10), 2051–2066. https://doi.org/10.1111/maps.13107

Gounelle, M., Chaussidon, M., Morbidelli, A., Barrat, J. A., Engrand, C., Zolensky, M. E., & McKeegan, K. D. (2009). A unique basaltic micrometeorite expands the inventory of solar system planetary crusts. *Proceedings of the National Academy of Sciences*, *106*(17), 6904–6909. https://doi.org/10.1073/pnas.0900328106

Höfle, H. C. (1989). The glacial history of the Outback Nunataks area in western North Victoria Land. *Geologisches Jahrbuch*, (38), 335–355.

Kurat, G., Koeberl, C., Presper, T., Brandstätter, F., & Maurette, M. (1994). Petrology and geochemistry of Antarctic micrometeorites. *Geochimica et Cosmochimica Acta*, *58*(18), 3879–3904. https://doi.org/10.1016/0016-7037(94)90369-7

Love, S. G., & Brownlee, D. E. (1991). Heating and thermal transformation of micrometeoroids entering the Earth's atmosphere. *Icarus*, *89*(1), 26–43. https://doi.org/10.1016/0019-1035(91)90085-8

Love, S. G., & Brownlee, D. E. (1993). A direct measurement of the terrestrial mass accretion rate of cosmic dust. *Science*, *262*(5133), 550–553. https://doi.org/10.1126/science.262.5133.550

Marzari, F., & Vanzani, V. (1994). Orbital evolution of dust particles near mean motion resonances with the Earth. *Planetary and Space Science*, *42*(2), 101–110. https://doi.org/10.1016/0032-0633(94)90017-5

McLachlan, G. J., & Peel, D. (2000). *Finite mixture models*. John Wiley & Sons. https://doi.org/10.1002/0471721182

Nava, J., Suttle, M. D., Spiess, R., Folco, L., Najorka, J., Carli, C., & Massironi, M. (2020). Hydrothermal activity on the CV parent body: New perspectives from the giant Transantarctic Mountains minimeteorite TAM 5.29. *Meteoritics & Planetary Science*, *55*(1), 164–183. https://doi.org/10.1111/maps.13429

Nishiizumi, K., Kohl, C. P., Arnold, J. R., Klein, J., Fink, D., & Middleton, R. (1991). Cosmic ray produced 10Be and 26Al in Antarctic rocks: Exposure and erosion history. *Earth and Planetary Science Letters*, *104*(2-4), 440–454. https://doi.org/10.1016/0012-821X(91)90221-3

Noguchi, T., Ohashi, N., Tsujimoto, S., Mitsunari, T., Bradley, J. P., Nakamura, T., et al. (2015). Cometary dust in Antarctic ice and snow: Past and present chondritic porous micrometeorites preserved on the Earth's surface. *Earth and Planetary Science Letters*, *410*, 1–11. https://doi.org/10.1016/j.epsl.2014.11.012

Ottaviani, S. (2026). Cosmic Dust Flux During the Quaternary: The Record of Large Scoriaceous and Unmelted Micrometeorites from the Transantarctic Mountains Collection [Dataset]. *Zenodo*. https://doi.org/10.5281/zenodo.20184378

Paganin, D., Mayo, S. C., Gureyev, T. E., Miller, P. R., & Wilkins, S. W. (2002). Simultaneous phase and amplitude extraction from a single defocused image of a homogeneous object. *Journal of microscopy*, *206*(1), 33–40. https://doi.org/10.1046/j.1365-2818.2002.01010.x

Prasad, M. S., Rudraswami, N. G., & Panda, D. K. (2013). Micrometeorite flux on Earth during the last∼ 50,000 years. *Journal of Geophysical Research: Planets*, *118*(11), 2381–2399. https://doi.org/10.1002/2013JE004460

Rochette, P., Folco, L., Suavet, C., Van Ginneken, M., Gattacceca, J., Perchiazzi, N., et al. (2008). Micrometeorites from the transantarctic mountains. *Proceedings of the National Academy of Sciences*, *105*(47), 18206–18211. https://doi.org/10.1073/pnas.0806049105

Rojas, J., Duprat, J., Engrand, C., Dartois, E., Delauche, L., Godard, M., et al. (2021). The micrometeorite flux at Dome C (Antarctica), monitoring the accretion of extraterrestrial dust on Earth. *Earth and Planetary Science Letters*, *560*, 116794. https://doi.org/10.1016/j.epsl.2021.116794

Rubin, A. E., & Grossman, J. N. (2010). Meteorite and meteoroid: New comprehensive definitions. *Meteoritics & Planetary Science*, *45*(1), 114–122. https://doi.org/10.1111/j.1945-5100.2009.01009.x

Rudraswami, N. G., Prasad, M. S., Babu, E. V. S. S. K., Kumar, T. V., Feng, W., & Plane, J. M. C. (2012). Fractionation and fragmentation of glass cosmic spherules during atmospheric entry. *Geochimica et Cosmochimica Acta*, *99*, 110–127. https://doi.org/10.1016/j.gca.2012.09.036

Schultz, L., Annexstad, J. O., & Delisle, G. (1990). Ice movement and mass balance at the Allan Hills Icefield. *Antarctic Journal of the United States*, *25*(5), 94.

Shapiro, S. S., & Wilk, M. B. (1965). An analysis of variance test for normality (complete samples). *Biometrika*, *52*(3-4), 591–611. https://doi.org/10.1093/biomet/52.3-4.591

Soens, B., Chernonozhkin, S. M., de Vega, C. G., Vanhaecke, F., Van Ginneken, M., Claeys, P., & Goderis, S. (2022). Characterization of achondritic cosmic spherules from the Widerøefjellet micrometeorite collection (Sør Rondane Mountains, East Antarctica). *Geochimica et Cosmochimica Acta*, *325*, 106–128. https://doi.org/10.1016/j.gca.2022.03.029

Suavet, C., Alexandre, A., Franchi, I. A., Gattacceca, J., Sonzogni, C., Greenwood, R. C., et al. (2010). Identification of the parent bodies of micrometeorites with high-precision oxygen isotope ratios. *Earth and Planetary Science Letters*, *293*(3-4), 313–320. https://doi.org/10.1016/j.epsl.2010.02.046

Suavet, C., Gattacceca, J., Rochette, P., & Folco, L. (2011). Constraining the terrestrial age of micrometeorites using their record of the Earth's magnetic field polarity. *Geology*, *39*(2), 123–126. https://doi.org/10.1130/G31655.1

Suavet, C., Rochette, P., Kars, M., Gattacceca, J., Folco, L., & Harvey, R. P. (2009). Statistical properties of the Transantarctic Mountains (TAM) micrometeorite collection. *Polar Science*, *3*(2), 100–109. https://doi.org/10.1016/j.polar.2009.06.003

Suttle, M. D., Dionnet, Z., Franchi, I., Folco, L., Gibson, J., Greenwood, R. C., et al. (2020). Isotopic and textural analysis of giant unmelted micrometeorites–identification of new material from intensely altered 16O-poor water-rich asteroids. *Earth and Planetary Science Letters*, *546*, 116444. https://doi.org/10.1016/j.epsl.2020.116444

Suttle, M. D., & Folco, L. (2020). The extraterrestrial dust flux: Size distribution and mass contribution estimates inferred from the Transantarctic Mountains (TAM) micrometeorite collection. *Journal of Geophysical Research: Planets*, *125*(2), e2019JE006241. https://doi.org/10.1029/2019JE006241

Suttle, M. D., Folco, L., Genge, M. J., Russell, S. S., Najorka, J., & van Ginneken, M. (2019). Intense aqueous alteration on C-type asteroids: Perspectives from giant fine-grained micrometeorites. *Geochimica et cosmochimica acta*, *245*, 352–373. https://doi.org/10.1016/j.gca.2018.11.019

Suttle, M. D., Genge, M. J., Folco, L., & Russell, S. S. (2017). The thermal decomposition of fine-grained micrometeorites, observations from mid-IR spectroscopy. *Geochimica et Cosmochimica Acta*, *206*, 112–136. https://doi.org/10.1016/j.gca.2017.03.002

Suttle, M. D., Genge, M. J., Folco, L., Van Ginneken, M., Lin, Q., Russell, S. S., & Najorka, J. (2019). The atmospheric entry of fine-grained micrometeorites: The role of volatile gases in heating and fragmentation. *Meteoritics & Planetary Science*, *54*(3), 503–520. https://doi.org/10.1111/maps.13220

Suttle, M. D., Genge, M. J., & Russell, S. S. (2017). Shock fabrics in fine-grained micrometeorites. *Meteoritics & Planetary Science*, *52*(10), 2258–2274. https://doi.org/10.1111/maps.12927

Taylor, S., Lever, J. H., & Harvey, R. P. (1998). Accretion rate of cosmic spherules measured at the South Pole. *Nature*, *392*(6679), 899–903. https://doi.org/10.1038/31894

Taylor, S., Lever, J. H., & Harvey, R. P. (2000). Numbers, types, and compositions of an unbiased collection of cosmic spherules. *Meteoritics & Planetary Science*, *35*(4), 651–666. https://doi.org/10.1111/j.1945-5100.2000.tb01450.x

Taylor, S., Matrajt, G., & Guan, Y. (2012). Fine-grained precursors dominate the micrometeorite flux. *Meteoritics & Planetary Science*, *47*(4), 550–564. https://doi.org/10.1111/j.1945-5100.2011.01292.x

Toppani, A., & Libourel, G. (2003). Factors controlling compositions of cosmic spinels: Application to atmospheric entry conditions of meteoritic materials. *Geochimica et Cosmochimica Acta*, *67*(23), 4621–4638. https://doi.org/10.1016/S0016-7037(03)00383-1

Toppani, A., Libourel, G., Engrand, C., & Maurette, M. (2001). Experimental simulation of atmospheric entry of micrometeorites. *Meteoritics & Planetary Science*, *36*(10), 1377–1396. https://doi.org/10.1111/j.1945-5100.2001.tb01831.x

Van der Wateren, F. M., Dunai, T. J., Van Balen, R. T., Klas, W., Verbers, A. L., Passchier, S., & Herpers, U. (1999). Contrasting Neogene denudation histories of different structural regions in the Transantarctic Mountains rift flank constrained by cosmogenic isotope measurements. *Global and Planetary Change*, *23*(1-4), 145–172. https://doi.org/10.1016/S0921-8181(99)00055-7

Van der Wateren, F. M., Verbers, A. L. L. M., Luyendyk, B. P., Smith, C. H., Höfle, H. C., Vermeulen, F. J. M., et al. (1996). Glaciation and deglaciation of the uplifted margins of the Cenozoic west Antarctic rift system, Ross sea, Antarctica. *Geologisches Jahrbuch. Reihe B: Regionale Geologie Ausland*, *89*, 123–155.

van Ginneken, M., Folco, L., Cordier, C., & Rochette, P. (2012). Chondritic micrometeorites from the Transantarctic Mountains. *Meteoritics & Planetary Science*, *47*(2), 228–247. https://doi.org/10.1111/j.1945-5100.2011.01322.x

van Ginneken, M., Folco, L., Perchiazzi, N., Rochette, P., & Bland, P. A. (2010). Meteoritic ablation debris from the Transantarctic Mountains: Evidence for a Tunguska-like impact over Antarctica ca. 480 ka ago. *Earth and Planetary Science Letters*, *293*(1-2), 104–113. https://doi.org/10.1016/j.epsl.2010.02.028

van Ginneken, M., Gattacceca, J., Rochette, P., Sonzogni, C., Alexandre, A., Vidal, V., & Genge, M. J. (2017). The parent body controls on cosmic spherule texture: Evidence from the oxygen isotopic compositions of large micrometeorites. *Geochimica et Cosmochimica Acta*, *212*, 196–210. https://doi.org/10.1016/j.gca.2017.05.008

van Ginneken, M., Genge, M. J., Folco, L., & Harvey, R. P. (2016). The weathering of micrometeorites from the Transantarctic Mountains. *Geochimica et Cosmochimica Acta*, *179*, 1–31. https://doi.org/10.1016/j.gca.2015.11.045

van Ginneken, M., Wozniakiewicz, P. J., Brownlee, D. E., Debaille, V., Della Corte, V., Delauche, L., et al. (2024). Micrometeorite collections: A review and their current status. *Philosophical Transactions A*, *382*(2273), 20230195. https://doi.org/10.1098/rsta.2023.0195

Van Maldeghem, F., Van Ginneken, M., Soens, B., Kaufmann, F., Lampe, S., Ruggiu, L. K., et al. (2023). Geochemical characterization of scoriaceous and unmelted micrometeorites from the Sør Rondane Mountains, East Antarctica: Links to chondritic parent bodies and the effects of alteration. *Geochimica et Cosmochimica Acta*, *354*, 88–108. https://doi.org/10.1016/j.gca.2023.06.002

Walton, C. R., Rigley, J. K., Lipp, A., Law, R., Suttle, M. D., Schönbächler, M., et al. (2024). Cosmic dust fertilization of glacial prebiotic chemistry on early Earth. *Nature Astronomy*, *8*(5), 556–566. https://doi.org/10.1038/s41550-024-02212-z

Welten, K. C., Folco, L., Nishiizumi, K., Caffee, M. W., Grimberg, A., Meier, M., & Kober, F. (2008). Meteoritic and bedrock constraints on the glacial history of Frontier Mountain in northern Victoria Land, Antarctica. *Earth and Planetary Science Letters*, *270*(3-4), 308–315. https://doi.org/10.1016/j.epsl.2008.03.052